Reaction of 1,3-Butadiene with Electron-Rich Binuclear Rhodium Hydrides. New Bonding Modes for 1,3-Dienes to Two Metal Centers

Michael D. Fryzuk,*,† Warren E. Piers,†,‡ Steven J. Rettig,†,§ Frederick W. B. Einstein,*,∥ Terry Jones,∥ and Thomas A. Albright*,⊥

Contribution from the Department of Chemistry, University of British Columbia, 2036 Main Mall, Vancouver, BC Canada V6T 1Y6, Department of Chemistry, Simon Fraser University, Burnaby, BC Canada V5S 2N2, and Department of Chemistry, University of Houston, Houston, Texas 77204-5641. *Received July 22, 1988*

Abstract: The electron-rich binuclear rhodium hydrides $[\{Pr^i_2P(CH_2)_nPPr^i_2\}Rh]_2(\mu\text{-}H)_2$ (n = 3, **1a**; n = 2, **1b**) react with 1,3-butadiene to form complexes of the general formula $[\{Pr^i_2P(CH_2)_nPPr^i_2\}Rh]_2(C_4H_6)$. Thus, the major product in the reaction of **1a** with butadiene is the partial sandwich complex $[\{Pr^i_2P(CH_2)_3PPr^i_2\}Rh]_2(\mu\text{-}\eta^3\text{-}\eta^3\text{-}C_4H_6)$ (**2**) in which the 1,3-butadiene is bridging the two rhodium centers in a μ-η^3-η^3 bonding mode; also produced are mononuclear 1-methylallyl rhodium diphosphine diastereomers (syn:anti = 1:4). From the reaction of **1b** with 1,3-butadiene, only binuclear products are observed; in this case a mixture of two species is detected in solution, one of which has a C–H bond of the diene activated to generate $[\{Pr^i_2P(CH_2)_2PPr^i_2\}Rh]_2(\mu\text{-}H)(\mu\text{-}\eta^4\text{-}\sigma\text{-}C_4H_5)$ (**4a**), and the other is the analogue to **2**, $[\{Pr^i_2P(CH_2)_2PPr^i_2\}Rh]_2(\mu\text{-}\eta^3\text{-}\eta^3\text{-}C_4H_6)$ (**4b**). These two binuclear derivatives **4a** and **4b** are in the equilibrium in solution with ΔH° = 3.3 (1) kcal/mol and ΔS° = 8.5 (2) eu. The butadienyl–hydride complex **4a** is fluxional at room temperature, whereas both **2** and **4b** are static on the NMR time scale. Both **2** and **4a** have been characterized by X-ray crystallography; **2** crystallizes in the space group $C2/c$ (a = 25.583 (3) Å, b = 10.883 (1) Å, c = 14.602 (2) Å, V = 4058.9 (8) Å^3, Z = 4); least-squares refinement led to a value of R = 0.033 ($I \geq 3\sigma(I)$, 2687 reflections). **4a** crystallizes in the space group $P\bar{1}$ (a = 12.505 (1) Å, b = 17.627 (1) Å, c = 17.865 (3) Å, V = 3835.31 Å^3, Z = 4); least-squares refinement led to value of R = 0.037 ($I \geq 3\sigma(I)$, 7028 reflections). A proposal for the mechanism of formation of these complexes is presented based on the observation of an η^2-butadiene intermediate at low temperature and labeling studies involving the reactions of the dideuterated dimers **1a**-d_2 and **1b**-d_2 with 1,3-butadiene; also important is the reaction of the chloride-bridged dimers $[\{Pr^i_2P(CH_2)_nPPr^i_2\}Rh]_2(\mu\text{-}Cl)_2$ with "magnesium butadiene", $(Mg{\cdot}C_4H_6{\cdot}2THF)_n$, which generates the same binuclear products, thus suggesting that there is a common mechanism. Extended Hückel molecular orbital calculations on the bonding of the "partial sandwich" dimer show that the μ-η^3-η^3 bonding description results from a Jahn–Teller distortion from μ-η^4-η^4 "full sandwich" bonding; the optimized μ-η^3-η^3 form was found to be 48.7 kcal/mol more stable than the μ-η^4-η^4 form. However, this μ-η^4-η^4 description is more stable for the theoretical molecule $[(R_3P)_2Rh]_2(\mu\text{-}C_4H_4)$.

Much of our understanding of the interaction of unsaturated hydrocarbon ligands with transition metals arises from structural and theoretical studies on mononuclear complexes.[1] From these studies, both molecular-orbital bonding schemes for the metal–π-ligand interaction and a protocol for predicting[2] reactive sites on that coordinated π-system are available for most unsaturated hydrocarbon moieties. With polynuclear complexes on the other hand, much less is known about the activation of unsaturated hydrocarbons. In fact, we are rarely able to predict a priori the binding modes of π-type hydrocarbons to metal clusters, let alone sites of reactivity. However, a particularly attractive premise that has grown out of polynuclear cluster chemistry[3] is that new ways to activate unsaturated hydrocarbon fragments may be possible if binding to two or more metal centers is achieved.

1,3-Butadiene is a good case in point. This simple acyclic conjugated diene normally binds to mononuclear transition-metal centers in the η^4-cis mode as in I.[4] More recently, the η^4-trans

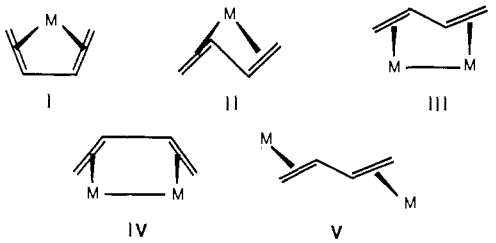

I II III IV V

form II has been observed as the kinetic product[5] in group 4 metallocenes and as the most stable isomer[6] in $(\eta^5\text{-}C_5H_5)MoNO(\eta^4\text{-}C_4H_6)$. Certainly in complexes of the type I, reactivity patterns are predictable. With polynuclear metal complexes, the s-trans bridging mode III has been characterized[7] as one of the possible binding modes for 1,3-butadiene; for example[7a], type III was found in $Os_3(CO)_{10}(\mu\text{-}\eta^2\text{-}\eta^2\text{-}C_4H_6)$ along with $Os_3(CO)_{10}(\eta^4\text{-}C_4H_6)$, which exhibits type I binding. The s-cis μ-η^2-η^2 bridging mode IV is known[8] for $Cp_2Co_2(\mu\text{-}CO)(\mu\text{-}\eta^2\text{-}\eta^2\text{-}C_4H_6)$; in addition, μ-η^2-η^2 bonding of butadiene in the absence of metal–metal interaction (type V) has been observed[9,10] in $Cp_2Mn_2(CO)_4(\mu$-

† University of British Columbia.
‡ NSERC Postgraduate Scholar (1984–1988).
§ Experimental Officer: UBC Crystallographic Service.
∥ Simon Fraser University.
⊥ University of Houston.

(1) (a) Albright, T. A.; Burdett, J. K.; Whangbo, M. H. *Orbital Interactions in Chemistry*; Wiley: New York, 1985. (b) Yamamoto, A. *Organotransition Metal Chemistry*; Wiley: New York, 1986; pp 57–75.
(2) Hegedus, L. S. In *The Chemistry of the Metal–Carbon Bond*; Hartley, F. R., Patai, S., Eds.; Wiley: New York, 1985; Vol. 2, p 401.
(3) (a) See for example: Muetterties, E. L.; Burch, R. R.; Shustermann, A. J.; Teller, R. G.; Williams, J. M. *J. Am. Chem. Soc.* **1983**, *105*, 3546. (b) Krause, M. J.; Muetterties, E. L. *Angew. Chem., Int. Ed. Engl.* **1983**, *22*, 135–48.
(4) Marr, G.; Rockett, B. W. In *The Chemistry of the Metal-Carbon Bond*; Hartley, F. R., Patai, S., Eds.; Wiley: New York, 1982; Vol. 1, Chapter 9, p 237, and references therein.
(5) (a) Erker, G.; Wicher, J.; Engl, K.; Rosenfeldt, F.; Dietrich, W.; Kruger, C. *J. Am. Chem. Soc.* **1980**, *102*, 6346. (b) Dorf, U.; Erker, G. *Organometallics* **1983**, *2*, 462. (c) Czisch, P.; Erker, G.; Korth, H.; Sustmann, R. *Organometallics* **1984**, *3*, 945. (d) Yasuda, H.; Kajihara, Y.; Mashima, K.; Nagasuna, K.; Lee, K.; Nakamura, A. *Organometallics* **1982**, *1*, 338.
(6) (a) Hunter, A. D.; Legzdins, P.; Nurse, C. R.; Einstein, F. W. B.; Willis, A. C. *J. Am. Chem. Soc.* **1985**, *107*, 1791. (b) Hunter, A. D. Ph.D. Thesis, University of British Columbia, 1986.
(7) (a) Tachikawa, M.; Shapley, J. R.; Haltiwanger, R. C.; Pierpoint, C. G. *J. Am. Chem. Soc.* **1976**, *98*, 4651. (b) Franzreb, K.-H.; Kreiter, C. G. *Z. Naturforsch., B* **1982**, *37B*, 1058. There are also examples of Type III bonding in the absence of a metal–metal interaction: (c) Ziegler, M. *Z. Anorg. Allg. Chem.* **1967**, *355*, 12. (d) Adams, V. C.; Jarvis, J. A. J.; Kilbourne, B. T.; Owston, P. G. *J. Chem. Soc. D* **1971**, 467.
(8) Vollhardt, K. P. C.; King, J. A., Jr. *Organometallics* **1983**, *2*, 684.

0002-7863/89/1511-5709$01.50/0

η^2-η^2-C_4H_6) and $[NMe_3Et]^+_2[Pt_2Cl_6(\mu$-$\eta^2$-$\eta^2$-$C_4H_6)]^{2-}$. It is reasonable to suggest that all five modes of binding activate 1,3-butadiene in different ways, and types III–V are only possible with two or more metal centers proximate.

In this paper we present the results of a study of the reaction of 1,3-butadiene with two electron-rich, binuclear rhodium hydrides of the general formula $[P_2Rh]_2(\mu$-$H)_2$ [**1a**, P_2 = 1,3-bis-

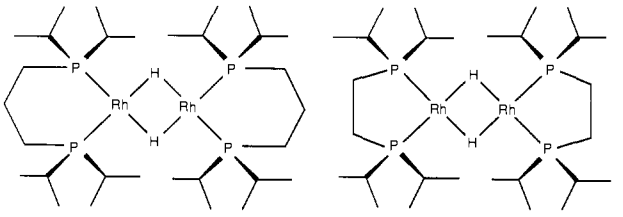

1a **1b**

$[(dippp)Rh]_2(\mu$-$H)_2$ $[(dippe)Rh]_2(\mu$-$H)_2$

(diisopropylphosphino)propane (dippp); **1b**, P_2 = 1,2-bis(diisopropylphosphino)ethane (dippe)]. Although the only difference between these two starting dihydrides **1a** and **1b** is the size of the chelate ring in the ancillary bidentate phosphine ligand, the product distribution upon reaction with 1,3-butadiene varies remarkably; however, in each case a binuclear compound is obtained that coordinates 1,3-butadiene in an alternate binding mode to **III–V**. In an effort to understand these unusual products, a mechanism for their formation is presented along with theoretical studies at the extended Hückel level on the nature of the binding of an intact 1,3-butadiene to two metal centers. Part of this work has been communicated previously.[11,12]

Experimental Section

General Procedures. All manipulations were performed under prepurified dinitrogen in a Vacuum Atmospheres HE-553-2 glovebox equipped with a MO-40-2H purifier, or in standard Schlenk-type glassware. The description "reactor bomb" refers to a cylindrical, thick-walled Pyrex vessel equipped with a 5-mm Kontes needle valve and a ground glass joint for attachment to a vacuum line. Larger bombs have 10-mm Kontes valves.

Hydrated rhodium trichloride was obtained from Johnson-Matthey and used as received to prepare $[(COD)RhCl]_2$[13a] (COD = 1,5-cyclooctadiene) and $[(COE)_2RhCl]_2$[13b] (COE = cyclooctene) by literature methods. (η^3-C_3H_5)Rh(COD) was also prepared via a literature procedure[14] and was used as an orange oil, without purification by sublimation, to prepare the dihydrides $[\{Pr^i_2P(CH_2)_nPPr^i_2\}Rh]_2(\mu$-$H)_2$ [n = 3, $[(dippp)Rh]_2(\mu$-$H)_2$ (**1a**); n = 2, $[(dippe)Rh]_2(\mu$-$H)_2$ (**1b**)] by literature procedures;[15,16] the dideuterides **1a**-d_2 and **1a**-d_2 were prepared similarly. 1,3-Butadiene was obtained from Matheson Gas Products and used from the cylinder by condensing into a reactor bomb and vacuum transferring from a −10 °C bath. $[Mg(C_4H_6)\cdot 2THF]_n$ was prepared by a literature method.[17]

Toluene and diethyl ether (Et_2O) were purified by distillation from sodium–benzophenone ketyl under argon. Tetrahydrofuran (THF) and hexanes were predried by refluxing over calcium hydride followed by distillation from sodium–benzophenone ketyl under argon.

Melting points were determined on a Mel-Temp apparatus in sealed capillaries under nitrogen and are uncorrected. Carbon, hydrogen, and halogen analyses were performed by Mr. P. Borda of this department. ^1H NMR spectral measurements were carried out on one of the following instruments: Varian XL-300, Bruker WP-80, or a Bruker WH-400. (All $^1H\{^{31}P\}$ spectra were obtained from the Bruker WH-400.) $^{31}P\{^1H\}$ NMR measurements were carried out at 121.421 MHz on the Varian XL-300, using trimethyl phosphite as an external standard (141.0 ppm). $^{13}C\{^1H\}$ spectra were run at 75.429 MHz, also on the Varian instrument, using internal solvent peaks as a reference (C_6D_6, 128.0 ppm). NMR solvents C_6D_6 and C_7D_8 were bought from MSD Isotopes, dried over activated 3-Å molecular sieves, and vacuum transferred, while THF-d_8 was dried over sodium–benzophenone ketyl, and stored under dry nitrogen. Simulated NMR spectra were obtained with the program PANIC.[18]

Synthesis of $[(dippp)Rh]_2(\mu$-$Cl)_2$ (5a). To a vigorously stirred suspension of $[(COE)_2RhCl]_2$ (0.50 g, 0.70 mmol) in hexanes (50 mL) was added in one portion, a solution of 1,3-bis(diisopropylphosphino)propane (dippp, 0.39 g, 1.39 mmol) in hexanes (10 mL). The disappearance of all solid $[(COE)_2RhCl]_2$ along with a deepening of the orange coloring of the solution was followed by precipitation of the bright orange product. The product suspension was reduced in volume to 40 mL and cooled to −30 °C to complete product precipitation. The product was collected on a fine-porosity frit, and washed with three 15-mL portions of cold hexanes (0.55 g, 0.66 mmol, 95%). ^1H NMR (C_6D_6, ppm): CH(CH_3)$_2$, 2.12 (d sp, $^3J_{CH3}$ = 7.6 Hz, ^2J_P = 1.8 Hz); CH(CH_3)$_2$, 1.61, 1.10 (dd, ^3J_P = 14.8 Hz); $CH_2CH_2CH_2$, 1.51 (d p, $^2J_{CH2}$ = 4.8 Hz, ^3J_P = 18.0 Hz); $CH_2CH_2CH_2$, 0.83 (br m). $^{31}P\{^1H\}$ NMR (C_6D_6, ppm referenced to $P(OCH_3)_3$ at 141.0): 47.68 (d, J_{Rh} = 189.2 Hz). Anal. Calcd for $C_{30}H_{68}P_4Cl_2Rh_2$: C, 43.43; H, 8.28; Cl, 8.55. Found: C, 43.65; H, 8.36; Cl, 8.75.

Synthesis of $[(dippp)Rh]_2(\mu$-η^3-η^3-$C_4H_6)$ (2). Method A. $[(dippp)Rh]_2(\mu$-$H)_2$ (0.50 g, 0.66 mmol) was dissolved in toluene (40 mL), placed in a thick-walled reactor bomb, and attached to a vacuum line. The solution was degassed, and approximately 5 equiv of 1,3-butadiene (3.29 mmol, 509 mmHg in a 110-mL volume) was transferred under vacuum into the reaction vessel. The reaction was stirred at room temperature until the black-green to yellow-orange color change was complete (4 h). The solvent and excess butadiene were pumped away to produce an oily yellow-orange crystalline mass, from which 0.33 g (0.42 mmol, 63%) of **2** was obtained upon recrystallization from toluene/hexanes, (1:2). mp: 178–179 °C dec. ^1H NMR (C_6D_6, ppm): H_c, 4.78 (m, $^3J_{cc'}$ = 4.45 Hz, $^3J_{ac}$ = 10.79 Hz, $^3J_{bc}$ = 6.60 Hz, $^4J_{b'c}$ = 1.45 Hz); H_b, 2.65 (m, $^2J_{ab}$ = 3.90 Hz); H_a, 0.87 (m, J_P = 4.0 Hz); CH(CH_3)$_2$, 2.24 (d sp, ^3J_H = 7.2 Hz, ^2J_P = 2.4 Hz), 2.08 (d sp, ^3J_H = 7.8 Hz), 1.78 (2 overlapping d sp, ^3J_H = ~6.4 Hz); $CH_2CH_2CH_2$, 1.90 (t p, ^3J_H = 4.8 Hz); $CH_2CH_2CH_2$, ~1.26 (m); CH(CH_3)$_2$, 1.52, 1.35, 1.12 (overlapping d d, ^3J_H = 6.4–7.8 Hz, ^3J_P = 12.0–14.4 Hz). $^{13}C\{^1H\}$ NMR (relative to C_6D_6 at 128.0 ppm): C_{int}, 60.2 (d, J_P = 18.0 Hz, ^1J_H = 156.0 Hz); C_{term}, 37.9 (d d, J_{Rh} = 10.0 Hz, J_P = 35.0 Hz, ^1J_H = 150.5, 149.8 Hz); ligand resonances, 17.5–29.0. $^{31}P\{^1H\}$ NMR (C_6D_6, ppm from external $P(OCH_3)_3$ set at 141.0): AA′BB′XX′ pattern, P_A, 54.4 ($^2J_{AB}$ = 40.5 Hz, J_{Rh} = 228.0 Hz); P_B, 36.0 (J_{Rh} = 180.4 Hz). Anal. Calcd for $C_{34}H_{74}P_4Rh_2$: C, 50.24; H, 9.19. Found: C, 49.99; H, 9.32. The nature of the 1-methylallyl byproducts was shown to be unambiguous through spectroscopic comparison with an authentic sample prepared by modification of a literature procedure.[19] An analytically pure sample could be obtained by sublimation of the residues obtained from the mother liquor of the above recrystallization at 10^{-4} mmHg and 70–80 °C to a probe cooled to −78 °C. Due to decomposition, the yield was 0.123 g (0.284 mmol, 21.5% based on starting material, syn:anti = 1:4). ^1H NMR (C_6D_6, ppm): H_a, 4.7 (m); H_b, 3.4 (br d, $^3J_{bc}$ = 7.2 Hz); H_d, 2.12 (dd, $^3J_{ac}$ = 12.2 Hz, $^2J_{ab}$ = 6.4 Hz); -CH_3, 1.22 (m); CH(CH_3)$_2$ and $CH_2CH_2CH_2$, 1.60–2.10; CH(CH_3)$_2$, 0.9–2.3 (overlapping dd). $^{13}C\{^1H\}$ NMR (C_6D_6, ppm): C_2, 101.6 (s); C_3, 60.4 (dd); C_1, 43.1 (ddd); CH_3, 24.3 (d). $^{31}P\{^1H\}$ NMR (C_6D_6, ppm referenced to $P(OCH_3)_3$ at 141.0): 45.5 (dd, J_{Rh} = 183.8 Hz, ^2J_P = 40.5 Hz); 40.0 (dd, J_{Rh} = 190.7 Hz).

Method B. To a THF (10-mL) suspension of $[(dippp)Rh]_2(\mu$-$Cl)_2$ (0.053 g, 0.064 mmol) cooled to −10 °C was added 1.1 equiv of $[Mg(C_4H_6)\cdot 2THF]_n$ (0.016 g, 0.072 mmol) suspended in 5.0 mL of THF. The reaction mixture was warmed to room temperature and stirred until clear (30 min), at which time the THF was removed under reduced pressure. The orange residues were extracted with hexanes and the extracts filtered through a Celite pad, resulting in a clear yellow solution. Upon slow evaporation of the hexanes 0.044 g (0.054 mmol, 84.7%) of spectroscopically pure yellow-orange crystals was obtained.

Synthesis of $[(dippe)Rh]_2(\mu$-$Cl)_2$ (5b). To a stirred suspension of $[(COE)_2RhCl]_2$ (0.25 g, 0.35 mmol) in toluene (40 mL) was added dropwise a solution of 1,2-bis(diisopropylphosphino)ethane (dippe; 0.18 g, 0.70 mmol) in 5 mL of toluene. The reaction was stirred for 15 min and the toluene removed under reduced pressure. The orange residues were recrystallized from toluene/hexanes (1:1), yielding orange crystals

(9) Ziegler, M. *Z. Anorg. Allg. Chem.* **1967**, *355*, 12.
(10) Adams, V. C.; Jarvis, J. A. J.; Kilbourne, B. T.; Owston, P. G. *J. Chem. Soc. D* **1971**, 467.
(11) Fryzuk, M. D.; Jones, T.; Einstein, F. W. B. *J. Chem. Soc., Chem. Commun.* **1984**, 1556.
(12) Fryzuk, M. D.; Piers, W. E.; Rettig, S. J. *J. Am. Chem. Soc.* **1985**, *107*, 8259.
(13) (a) Chatt, J.; Venanzi, L. M. *J. Chem. Soc.* **1957**, 4753. (b) van der Ent, A.; Onderdelinden, A. L. *Inorg. Synth.* **1973**, *14*, 93.
(14) Fryzuk, M. D.; Piers, W. E. *Organomet. Synth.* **1986**, *3*, 128.
(15) Fryzuk, M. D.; Piers, W. E.; Einstein, F. W. B.; Jones, T. *Can. J. Chem.*, in press.
(16) Fryzuk, M. D.; Jones, T.; Einstein, F. W. B. *Organometallics* **1984**, *3*, 184.
(17) Wreford, S. S.; Whitney, J. F. *Inorg. Chem.* **1981**, *20*, 3918.
(18) PANIC: Parameter Adjustment in NMR by Iteration Calculation. PANIC is a minicomputer version of larger LAOCOON-type programs used with the Bruker ASPECT 2000 software package.
(19) Fryzuk, M. D. *Inorg. Chem.* **1982**, *21*, 2134.

of **5a** (0.23 g 85.9%). ^{1}H NMR (C_6D_6, ppm): C*H*$(CH_3)_2$, 2.03 (d sp), ^3J_H = 7.6 Hz, ^2J_P = 1.8 Hz); CH$(CH_3)_2$, 1.50, 1.05 (dd, ^3J_P = 14.8 Hz), CH_2CH_2, 0.95 (m). ^{31}P{^{1}H} NMR (C_6D_6, ppm referenced to $P(OCH_3)_3$ at 141.0): 102.2 (d, J_{Rh} = 206.4 Hz).

Synthesis of [(dippe)Rh]$_2$(μ-H)(μ-η^4-σ-C_4H_5) (4a). Method A. [(dippe)Rh]$_2$(μ-H)$_2$ (0.100 g, 0.136 mmol) was dissolved in toluene (10 mL) and loaded into a small reactor bomb. An excess of 1,3-butadiene was condensed into the reaction vessel, and the reaction warmed gradually to room temperature. Near −78 °C, the characteristic deep green of the dihydride changed to an intense purple, which persisted until approximately −50 °C, at which time the solution began to turn orange. Before room temperature was reached, the color change was complete, and the toluene and excess 1,3-butadiene were removed in vacuo. The yellow-orange residue was recrystallized from toluene/hexanes, yielding 0.097 g of **4a**/**4b** (91%). Anal. Calcd for $C_{32}H_{70}P_4Rh_2$: C, 48.99, H, 8.99. Found: C, 49.03; H, 9.02. It appears that **4a** crystallizes preferentially, but in solution, a mixture of the two compounds is observed. Spectroscopic data for **4a**. ^{1}H NMR (C_6D_6, ppm, room temperature): diene protons, 6.48 (br m, 2 H); 2.65 (br m, 2 H); C*H*$(CH_3)_2$, 2.23 (br m, 2 H); 2.02 (d sp, ^3J_H = 7.0 Hz, 2 H); 1.83 (d sp, ^3J_H = 7.5 Hz, 2 H); 1.67 (br m, 2 H); CH$(CH_3)_2$, backbone, 0.69–1.50; Rh-*H*, −8.26 (br m, J_{Rh} = 26.7 Hz, t). ^{1}H NMR (C_7D_8, ppm, −70 °C): diene protons, 7.49 (br d, J = 16.6 Hz, 1 H); 5.56 (br s, 1 H); 2.8 (br s, 2 H); ligand resonances all broad, 0.60–2.60; Rh–H, −8.15 (br m). ^{31}P{^{1}H} NMR (C_6D_6, ppm referenced to $P(OCH_3)_3$ at 141.0, +40 °C): 101.88 (d, J_{Rh} = 163.7 Hz); 101.04 (d, J_{Rh} = 171.4 Hz). ^{31}P{^{1}H} NMR (C_7D_8, ppm referenced to $P(OCH_3)_3$ at 141.0, −80 °C): 3 overlapping signals at 101–105 (dd); 99.4 (dd, J_P = 25.5 Hz, J_{Rh} = 139.5 Hz (see text). ^{13}C{^{1}H} NMR (C_7D_8, ppm, −70 °C): Cσ(C_1), 156.9 (br m); C_2, 123.5 (br s); C_3, 88.8 (s); C_4, 33.1 (s); ligand resonances, 10.8–28.7. Spectroscopic data for **4b**. ^{13}C{^{1}H} NMR (C_6D_6, ppm): C_{int}, 63.24 (J_P = 19.8 Hz); C_{term}, 40.29 (J_{Rh} = 10.45 Hz, J_P = 36.45 Hz); ligand resonances, 21–32.

Method B. To a THF (10-mL) suspension of [(dippe)Rh]$_2$(μ-Cl)$_2$ (0.070 g, 0.087 mmol) cooled to −10 °C was added 1.1 equiv of [Mg(C_4H_6)·2THF]$_n$ (0.021 g, 0.096 mmol) suspended in 5.0 mL of THF. The reaction mixture was stirred at room temperature for 30 min, at which time the THF was removed under reduced pressure. The orange residues were extracted with hexanes and the extracts filtered through a Celite pad, resulting in a clear yellow-orange solution. Recrystallization from minimum hexanes at −20 °C yielded 0.055 g (0.070 mmol, 81.0%) of spectroscopically pure yellow-orange crystals of **4a**.

Observation of [(dippe)Rh]$_2$(μ-H)$_2$(η^2-C_4H_6), the Purple Intermediate. A solution of pure **1b** in C_7D_8 was placed in a sealable NMR tube and degassed on a vacuum line. The sample was then cooled to −78 °C in a dry-ice/acetone bath, and 3 equiv of 1,3-butadiene was transferred under vacuum into the sample tube. An immediate green to purple color change was observed; this purple species was stable for at least 8 h at −78 °C, and when the tube was transferred to an NMR probe precooled to −80 °C, ^{1}H, ^{13}C{^{1}H}, and ^{31}P{^{1}H} measurements could be obtained. ^{1}H NMR (C_7D_8, ppm, −80 °C): $H_{cent(unbound)}$, 6.12 (m, partially obscured by free butadiene resonances); $H_{trans(unbound)}$, 5.32 (br d, J = 16.4 Hz); $H_{trans(bound)}$, 4.45 (br m); $H_{cent(bound)}$, 4.08 (br m); $H_{cis(bound)}$, 2.85 (br m); $H_{cis(free)}$, 2.45 (br m); ligand resonances, 2.1–0.8 (br); Rh–H–Rh, −5.04 (m), −12.25 (m). ^{13}C{^{1}H} NMR (C_7D_8, ppm, −80 °C): diene resonances, 140.4 (s); 119.0 (s); 116.8 (s); 101.9 (s). ^{31}P{^{1}H} NMR (C_7D_8, ppm referenced to $P(OCH_3)_3$ at 141.0, −80 °C): 111.4 (ddd, $^1J_{Rh}$ = 174.3 Hz); 106.3 (dd, $^1J_{Rh}$ = 131.3 Hz, J_P = 21.3 Hz); 105.1 (dd, $^1J_{Rh}$ = 156.3, J_P = 30.4 Hz); 95.8 (br dd, $^1J_{Rh}$ = 122.0, J_P = 30.0 Hz).

Reaction of 1a-d_2 and 1b-d_2 with 1,3-Butadiene. A sample of either **1a**-d_2 or **1b**-d_2 (0.10 g) was dissolved in enough C_6D_6 for two NMR samples (5-mm tube, ≈1.2 mL) and placed in a small reactor bomb. 1,3-Butadiene (4 equiv) was condensed into the reaction vessel and the reaction allowed to occur. Upon completion, about half of the solution was transferred under vacuum to a sealable 5-mm NMR tube and the volatiles thus analyzed by ^{1}H and ^{2}H NMR. The remainder of the reacton solution, containing the organometallic products, was analyzed separately by the same techniques. No deuterium was detected in the binuclear organometallic products **2**, **4a**, or **4b**. The deuterium was found in the butenes produced in the reactions, as well as in the mononuclear 1-methylallyl complexes **3** produced in the reaction of **1b** and 1,3-butadiene.

Measurement of the Equilibrium between 4a and 4b. A 0.163 M solution of pure, crystalline [(dippe)Rh]$_2$·(C_4H_6) (0.064 g, 8.16×10^{-5} mol, 0.5 mL of C_7D_8) was sealed in a 5-mm NMR tube under ≈0.8 atm of N_2. The sample was placed in a thermostated probe for 15 min before pulsing began, and the phosphorus-31 spectra were collected as a function of temperature by using a 73° pulse, a 5-s relaxation delay, and broad-band proton decoupling. The isomer ratio was determined from each spectrum by integration of the appropriate peaks; no correction for NOE effects were made. The possibility of intensity anomalies due to relaxation time differences was ruled out when a separate experiment yielded T_1 values of between 2 and 3 for each phosphorus nucleus in the spectrum.

Table I. Crystallographic Data for **2** and **4a**

compound	**2**[a]	**4a**[b]
formula	$C_{34}H_{74}P_4Rh_2$	$C_{32}H_{70}P_4Rh_2$
fw	812.7	784.62
cryst system	monoclinic	triclinic
space group	$C2/c$	$P\bar{1}$
a, Å	25.583 (3)	12.505 (1)
b, Å	10.883 (1)	17.627 (1)
c, Å	14.602 (2)	17.865 (3)
α, deg	90	96.72 (1)
β, deg	93.259 (3)	90.44 (1)
γ, deg	90	101.14 (6)
V, Å^3	4058.9 (8)	3835.31
Z	4	4 (2 molecules per asymmetric unit)
D_{calcd}, g/cm^3	1.330	1.361
cryst dimens, mm	0.11 × 0.25 × 0.28	0.10 × 0.16 × 0.30
μ(Mo Kα), cm^{-1}	9.76	10.31
scan type	ω–2θ	ω–2θ
w scan speeds, deg min^{-1}	1.18–10.06	0.75–10.06
scan range (deg in ω)	0.75 + 0.35 tan θ	0.6 + 0.35 tan θ[c]
$2\theta_{max}$, deg	55	45
crystal decay	negligible	negligible
no. of unique reflctns	4643	9998
reflctns with $I \geq 3\sigma(I)$	2687	7028
R	0.033	0.037
R_w	0.035	0.048
no. of variables	197	695

[a] Temperature, 22 °C, Enraf-Nonius CAD4-F diffractometer, Mo Kα radiation ($\lambda K_{\alpha 1}$ = 0.709 30, $\lambda K_{\alpha 2}$ = 0.713 59 Å), graphite monochrometer, takeoff angle 2.7°, aperature (2.0 + tan θ) × 4.0 mm at a distance of 173 mm from the crystal, scan range extended by 25% on both sides for background measurement, $\sigma^2(I) = S + 2B + [0.04\,(S - B)]^2$ (S, scan count; B, normalized background count), function minimized $\sum w(|F_o| - |F_c|)^2$ where $w = 1/\sigma^2(F)$, $R = \sum||F_o| - |F_c||/\sum|F_o|$, $R_w = (\sum w(|F_o| - |F_c|)^2/\sum w|F_o|^2)^{1/2}$, $S = (\sum w(|F_o| - |F_c|)^2(m - n))^{1/2}$. Values given for R, R_w, and S are based on those reflections with $I \geq 3\sigma(I)$. [b] Temperature, 20 ± 1 °C; Mo Kα radiation, graphite monochromator, λ = 0.709 30 Å (α1), 0.713 59 Å (α2); function minimized: $\sum w(|F_o| - |F_c|)^2$ where $w = 1/\sigma^2(F) + 0.0006F^2$, $R = \sum||F_o| - |F_c||/\sum|F_o|$, $R_w = (\sum w(|F_o| - |F_c|)^2/\sum|F_o|)^{1/2}$. [c] The scan range was extended 25% on each side for background measurement.

X-ray Crystallographic Analysis of [(dippp)Rh]$_2$(μ-η^3-η^3-C_4H_6). Crystallographic data appear in Table I. Final unit-cell parameters were obtained by least-squares of 2 sin θ/λ values for 25 reflections with 2θ = 30–40°. The intensities of three standard reflections, measured each hour of X-ray exposure time throughout the data collection, showed only small random variations. Data were corrected for absorption by the Gaussian integration method.[20]

The centrosymmetric space group $C2/c$ was indicated by the E statistics and by the Patterson function, from which the Rh and P coordinates were determined. The remaining atoms were positioned from subsequent difference maps. The central carbon atom of the chelate ring (C(4)) was found to be twofold disordered. Site occupancy factors were estimated from relative Fourier peak heights and were adjusted to give nearly equal thermal parameters for each site. In the final stages of refinement the hydrogen atoms of the μ-η^3-η^3-C_4H_6 ligand and the low-occupancy disordered carbon atom, C(46), were refined with isotropic thermal parameters. The remaining non-hydrogen atoms were refined with anisotropic thermal parameters and the remaining full- and high-occupancy hydrogen atoms were fixed in idealized positions (C–H = 0.98 Å and $U_H \propto U_{Parent}$). Neutral atom scattering factors and anomalous scattering corrections (Rh, P) were taken from the standard source.[21] Final atomic coordinates and isotropic or equivalent isotropic (U_{eq} = $^1/_3$ trace U_{diag}) thermal parameters are given in Table II (supplementary

(20) The computer programs used include locally written programs for data processing and locally modified versions of the following: ORFLS, full-matrix least squares, and ORFFE, function and errors, by W. R. Busing, K. O. Martin, and H. A. Levy; FORDAP, Patterson and Fourier syntheses, by A. Zalkin; ORTEP II, illustrations, by C. K. Johnson; AGNOST, absorption corrections, by J. A. Ibers.

(21) *International Tables for X-ray Crystallography*; Kynoch Press: Birmingham, England, 1974; Vol. IV, pp 99–102, 149. (Present distributor, D. Riedel, Dordrecht, The Netherlands.)

Table VII. Parameters Used for the Extended Hückel Calculations

orbital		H_{ij}, eV	ζ_1	ζ_2	C_1[a]	C_2[a]
Rh	4d	−12.50	4.29	1.97	0.5807	0.5685
	5s	−8.09	2.135			
	5p	−4.57	2.10			
P	3s	−18.60	1.75			
	3p	−14.00	1.30			
C	2s	−21.40	1.625			
	2p	−11.40	1.625			
H	1s	−13.60	1.30			

[a] Contraction coefficients used in the double-ζ expansion.

material). Bond lengths and bond angles appear in Table III (supplementary material). Intraannular torsion angles, anisotropic thermal parameters, calculated hydrogen parameters, torsion angles, and measured and calculated structure factors are included as supplementary material.

X-ray Crystallographic Analysis of [(dippe)Rh]$_2$(μ-H)(μ-η^4-σ-C_4H_5) (4a). A red crystal was mounted in a thin-walled glass tube. Weissenberg photographs were used to determine the crystal system and assign the space group as $P1$ or $P\bar{1}$ (subsequent structure solution defined the space group as $P\bar{1}$). The crystal was then centered on an Enraf-Nonius CAD-4 diffractometer and accurate cell dimensions were determined by least-squares refinement of the setting angles of 25 accurately centered reflections (with $30.0° < 2\theta < 37.6°$) chosen from a variety of points in reciprocal space.

A total of 9998 independent reflections were measured, of which 7028 were classed observed [$I \geq 3\sigma(I)$] and used in subsequent structure solution and refinement. Lorentz, polarization, and analytical absorption corrections (transmission factors varied from 0.847 to 0.905) have been made.

The Rh atoms were located by using MULTAN, which showed there to be two dimeric molecules per asymmetric unit; all other non-hydrogen atoms were found in subsequent difference-Fourier maps. The vast majority of hydrogen atoms were found by difference synthesis; those not located were included in calculated positions. At this stage, all data were transferred to the CRYSTALS system[22] and refinement was continued by dividing the asymmetric unit into three batches; batch 1 consisted of the β-isopropyl carbons and hydrogens; batch 2 was made up of the methylene carbons, α-isopropyl carbons, and associated hydrogens; batch 3 contained Rh's, P's, hydride ligands, and butadienyl atoms. A number of block-matrix cycles were performed on each batch alternatively until the refinement had converged. During these cycles, in which all coordinates were refined, all alkyl hydrogen atoms were constrained[23] with respect to their parent carbon atoms [C–H = 0.95 (2) Å; C–C–H = 110 (2)°; H–C–H = 110 (2)°], all non-hydrogen atoms were given anisotropic temperature factors, and hydride ligands were given isotropic temperature factors and environmentally equivalent hydrogen atoms, e.g., those belonging to the same isopropyl group were given a collective isotropic temperature factor. Final cycles of block–diagonal least-squares refinement were performed with all alkyl hydrogen atoms included as fixed contributions, hydride ligands refined with isotropic temperature factors and non-hydrogen atoms with anisotropic parameters, agreement factors converged at $R = 0.037$ and $R_w = 0.048$ for 695 variables. Weights were divided on the basis of trends $w\Delta^2$ as a function of $\sin\theta/\lambda$ and F_o (Table I). Atomic scattering factors including anomalous dispersion were taken from tables for X-ray crystallography.[21] Final positional and thermal parameters are given in Table IV (supplementary material). Bond lengths and bond angles appear in Table VI (supplementary material). Anisotropic thermal parameters, hydrogen parameters and structure factor listings have been included as supplementary material.

Data reduction and initial structure solution were performed by the NRC VAX crystal structure system,[24] whereas the latter stages of structure solution and refinement were carried out with CRYSTALS.[22] All calculations were performed with an "in-house" VAX 750 computer.

Theoretical Computations. The extended Hückel calculations[25a] utilized a modified version of the Wolfsberg–Helmholtz formula.[25b] The parameters are listed in Table VII. All Rh–P, P–H, C–C, and C–H distances were held constant at 2.22, 1.41, 1.44, and 1.09 Å, respectively. The P–Rh–P and Rh–P–H angles were fixed at 97.0 and 125.26°, respectively. For the butadiene ligand C–C–C and C–C–H angles were idealized at 120.0°. In [$(PH_3)_2Rh]_2(\mu$-C_4H_6) and [$(PH_3)_2Rh]_2(\mu$-C_4H_4) the distance of Rh to the plane of the butadiene and cyclobutadiene ligands was held constant at 1.94 Å.

Scheme I

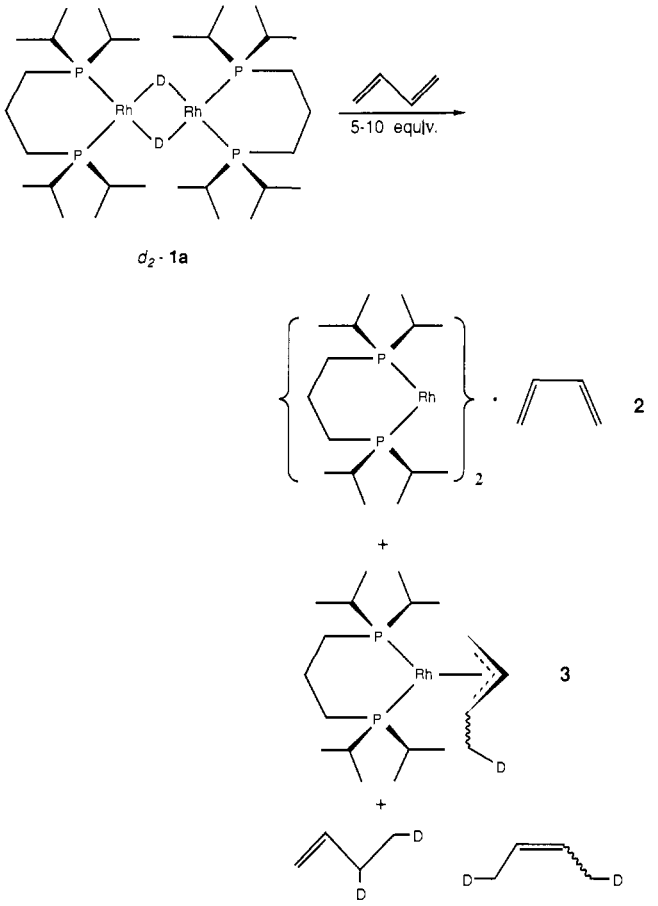

Results and Discussion

Reaction of [(dippp)Rh]$_2$(μ-H)$_2$ with 1,3-Butadiene. The addition of 5–10 equiv of 1,3-butadiene to the dippp dimer **1a** in toluene at room temperature results in a gradual color change from deep green to orange over a period of 1–2 h. The major product (50–60%) has the formula [(dippp)Rh]$_2$·C_4H_6 (**2**) and is obtained as orange crystals from toluene/hexanes at −30 °C. Also produced in this reaction is a syn/anti mixture of the mononuclear 1-methylallyl derivatives (η^3-1-MeC_3H_4)Rh(dippp) (**3**) in 20–25% isolated yield after sublimation. By $^{31}P\{^1H\}$ NMR spectroscopy, these are the only two organometallic products generated in the reaction. The ratio of the binuclear complex **2** to the mononuclear derivatives **3** varies from about 2:1 to 1:1 depending on the amount of 1,3-butadiene used; low ratios of 1,3-butadiene to the dippp dimer **1a** favor the binuclear complex **2**. The organic byproducts are a mixture of 1-butene, *cis*-butene, *trans*-butene (4:3:1), corresponding to 1 equiv based on **2**. The reaction of the dideuteride dimer **1a**-d_2 with 1,3-butadiene was also examined; no incorporation of deuterium into the binuclear complex **2** was detected by ^2H NMR spectroscopy. Deuterium label was detected in the butene byproducts and in the allyl complexes as shown in Scheme I.

The ^1H NMR spectrum of **2** consists of three multiplets for the butadiene ligand (see Experimental Section) and a set of resonances for the dippp ligand, which is complex but typical of some symmetry in the compound. The $^{31}P\{^1H\}$ NMR spectrum is of an AA′BB′XX′ spin system, which indicates that the phosphorus donors of each dippp ligand are inequivalent but both dippp ligands are symmetry related; this pattern is quite char-

(22) Watkin, D. CRYSTALS, Crystallographic suite. Chemical Crystallography Laboratory, Oxford University, 9 Parks Road, Oxford, England.
(23) Wasser, J. *Acta Crystallogr.* **1963**, *16*, 1091.
(24) Larson, A. C.; Lee, F. L.; Lepage, Y.; Gabe, E. J. The N.R.C. VAX Crystal Structure System. Chemistry Division, NRC, Ottawa, Ontario, Canada.
(25) (a) Hoffmann, R.; Lipscomb, W. N. *J. Chem. Phys.* **1962**, *36*, 2179, 3489; **1962**, *37*, 2872. Hoffmann, R. *Ibid.* **1963**, *39*, 1397. (b) Ammeter, J. H.; Bürgi, H.-B.; Thibeault, J. C.; Hoffmann, R. *J. Am. Chem. Soc.* **1978**, *100*, 3686.

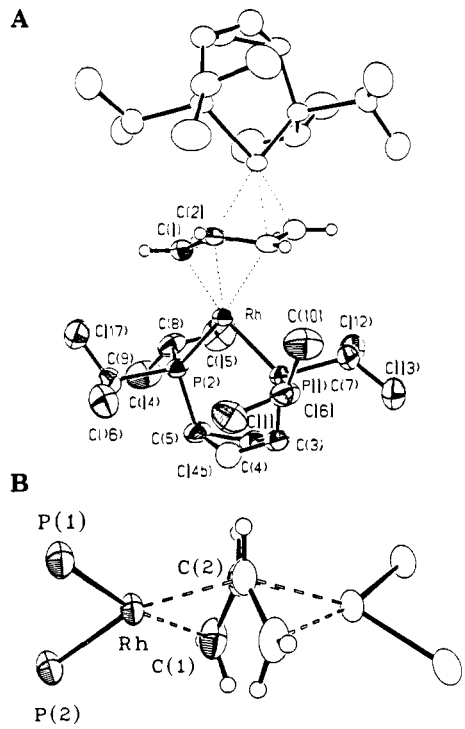

Figure 1. (A) ORTEP drawing and numbering scheme for the partial sandwich complex $[(dippp)Rh]_2(\mu\text{-}\eta^3\text{-}\eta^3\text{-}C_4H_6)$ **2**, looking down the C_2 axis. (B) Side view of **2** looking down the C(2)–C(2′) axis.

acteristic and serves as a useful diagnostic for this particular type of binuclear complex incorporating 1,3-butadiene. From the spectroscopic data alone, it was not possible to determine the exact structure and binding mode of the butadiene moiety; however, it was clear that the C_4H_6 fragment was intact (i.e., none of the C–H bonds had been cleaved) and that the diene itself was cis bound ($J_{H_{c,c'}}$ = 4.5 Hz).[26]

Solid-State Molecular Structure of $[(dippp)Rh]_2{\cdot}C_4H_6$. The single-crystal X-ray analysis of **2** showed that the 1,3-butadiene was indeed intact and *partially sandwiched* between the two rhodium centers (Figure 1). Each rhodium interacts in a η^3 fashion with the opposite faces of the twisted *cis*-1,3-butadiene fragment [torsion angle of 45.0 (8)°]. Table III lists bond lengths and bond angles (supplementary material). The rhodium dippp moieties are not unusual; the P(1)–Rh–P(2) angle of 96.96° is within the normal range expected[27] for six-membered chelate rings. The two [Rh(dippp)] units are skewed with respect to each other, as shown in Figure 1b; the dihedral angle formed by the two planes defined by the Rh, P(1), and P(2) atoms is 75.6 (1)°. The Rh–Rh separation of 4.1238 (6) Å is consistent with the presence of the bridging, partially sandwiched C_4H_6 unit inserted between the two metals.[28]

The dimensions associated with the inner core of this binuclear complex provide some insight into the bonding of this molecule. The carbon–carbon bond lengths of the C_4H_6 fragment are virtually identical at 1.44 Å [C(1)–C(2), 1.438 (7); C(2)–C(2′), 1.441 (9) Å] and are slightly longer than 1.40 Å as found in an η^3-cyclooctenyl rhodium derivative.[29] The C–C bond lengths found in $RhCl(\eta^4\text{-}C_4H_6)_2$ are 1.45 Å for C–C(internal) and 1.38 Å for C–C(external).[30] The diene unit is also twisted about the C(2)–C(2′) bond with a torsion angle of 45.0 (8)°. The rhodium–carbon distances reveal that the η^3 binding mode is asymmetric on each face; Rh–C(1) is 2.139 Å, Rh–C(2) is 2.208 Å, and Rh–C(2′) is 2.297 Å.

Table VIII. ^1H and $^{13}C\{^1H\}$ NMR Chemical Shift Comparison (ppm) between *anti*-**3**, **2**, and the Indicated Transition-Metal 1,3-Butadiene Complexes

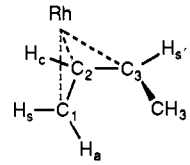

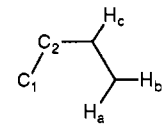

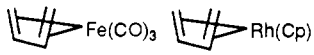

anti-**3**		**2**			
			^1H NMR		
H_a	2.12	H_a	0.87	−0.03	0.34
H_s	3.37	H_b	2.65	1.46	2.45
$H_{s'}$	4.45				
H_c	4.73	H_c	4.78	4.89	4.92
			^{13}C NMR		
C_1	43.1	C_1	37.9	40.53	
C_2	101.6	C_2	60.2	85.49	
C_3	60.4				

Solution-State Molecular Structure of $[(dippp)Rh]_2{\cdot}C_4H_6$. The solution spectroscopic data for **2** are consistent with the solid-state, partially sandwiched structure; however, the ^1H and $^{13}C\{^1H\}$ NMR chemical shifts of the diene protons in **2** are more typical of a cis η^4-1,3-butadiene structure than the observed η^3 type structure observed. Table VIII illustrates this by comparison of the spectroscopic data of **2** to that of the anti isomer of **3** as well as $(\eta^4\text{-}C_4H_6)Fe(CO)_3$[31] and the rhodium(I)–butadiene complex $(\eta^4\text{-}C_4H_6)RhCp$.[32] In particular, the chemical shift for the protons H_a, trans to the vicinal protons H_c, is indicative of an s-cis butadiene ligand. These protons characteristically resonate upfield in the 0.5–1.0 ppm region, whereas in Rh(I)–allyl complexes such as *anti*-**3**, the anti proton H_a resonates above 2.0 ppm. This high-field shift for H_a is also characteristic of an s-cis bound diene ligand; in an s-trans configuration, resonances for protons H_a are shifted to lower field (for example, δH_a = 1.43 ppm in $Os_3(CO)_{10}(\mu\text{-}\eta^2\text{-}\eta^2\text{-}C_4H_6)$).[7a] The $^{13}C\{^1H\}$ NMR of **2** also supports solution η^4 bonding, in that the resonance for C(2) is much closer in chemical shift to a diene C(2) carbon than C(2) in anti-**3**. Before engaging in a detailed discussion as to the nature of the bonding in solution of the diene ligand in **2** (vide infra), we point out that it must be quite rigid, because the ^1H and the $^{31}P\{^1H\}$ NMR spectra of **2** are *not* temperature dependent in the range −80 to +160 °C.

Reaction of $[(dippe)Rh]_2(\mu\text{-}H)_2$ with 1,3-Butadiene. The reaction of 1,3-butadiene (≥2 equiv) with the dippe hydride dimer **1b** proceeds very rapidly even at −10 °C, as evidenced by the color change from dark green to bright orange; yellow crystals of the formula $[(dippe)Rh]_2{\cdot}C_4H_6$ (**4**) can be isolated in >90% yield from toluene/hexanes at −30 °C. In contrast to the previous reaction of the dippp hydride dimer **1a** with 1,3-butadiene, binuclear products predominate to virtual exclusivity with **1b** and 1,3-butadiene; only traces of the mononuclear 1-methylallyl complexes $(\eta^3\text{-}1\text{-}MeC_3H_4)Rh(dippe)$ (**5**) are detectable (<1% by $^{31}P\{^1H\}$ NMR spectroscopy). Also produced in this reaction is 1 equiv of 1-butene based on the starting dimer **1b**. In analogy to the dippp dimer reaction, the dippe dideuteride **1b**-d_2 generates **4** with no evidence of deuterium labeling in the dirhodium product; all of the deuterium is incorporated in the 1-butene in the 3,4-positions (Scheme II).

The ^1H and $^{31}P\{^1H\}$ NMR spectra of **4** are complex and temperature dependent to the extent that unambiguous assignment of its structure by these spectroscopic methods was not possible. However, single crystals were obtained from the reaction mixture and subjected to X-ray analysis (vide infra); only by combining

(26) (a) A coupling of 3–5 Hz between these magnetically inequivalent nuclei is typical for complexes in which the diene ligand is cis-bound.[26b] (b) Crews, P. *J. Am. Chem. Soc.* **1973**, *95*, 636.

(27) James, B. R.; Mahayan, D.; Williams, G. M.; Rettig, S. J. *Organometallics* **1983**, *2*, 1452.

(28) The upper limit on a Rh–Rh bond is probably ca. 3.2 Å. See: Cowie, M.; Dwight, S. K. *Inorg. Chem.* **1980**, *19*, 209, and references therein.

(29) Vitulli, G.; Raffaelli, A.; Costantino, P. A.; Barberini, C.; Marchetti, F.; Merlino, S.; Skell, P. S. *J. Chem. Soc., Chem. Commun.* **1983**, 232.

(30) Allegra, G.; Immirzi, I. *Acta Crystallogr.* **1969**, *B25*, 120.

(31) Data for $(C_4H_6)Fe(CO)_3$: Bachmann, K.; von Philipsborn, W. *Org. Magn. Reson.* **1976**, *8*, 648.

(32) Data for $[(C_4H_6)Rh(Cp)$: Nelson, S. M.; Sloan, M.; Drew, M. G. B. *J. Chem. Soc., Dalton Trans.* **1973**, 2195.

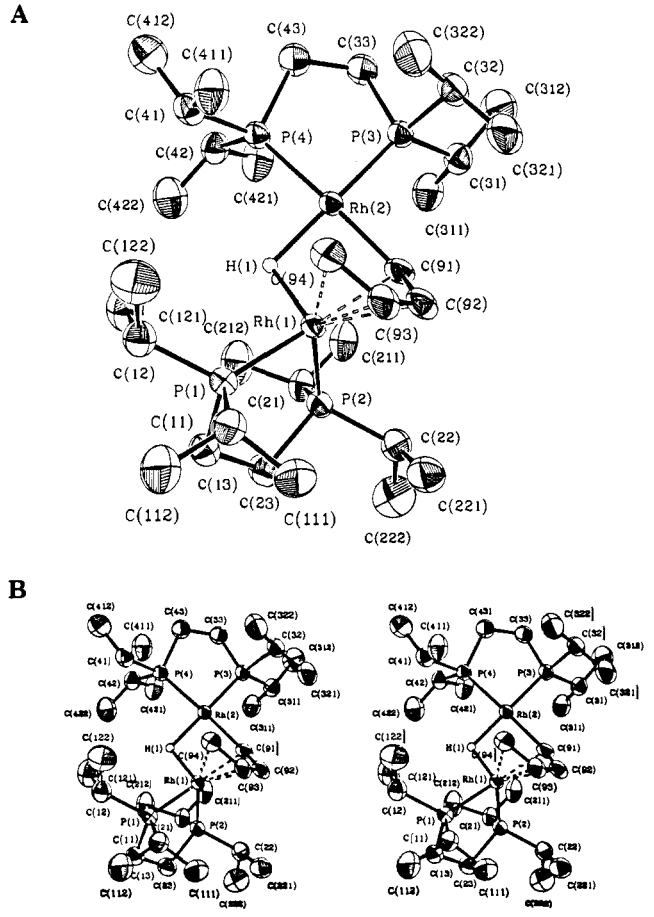

Figure 2. (A) ORTEP drawing and numbering scheme for the butadienyl-hydride complex $[(dippe)Rh]_2(\mu\text{-}\eta^4\text{-}\sigma\text{-}C_4H_5)(\mu\text{-}H)$ (**4a**). (B) Stereoview of the molecule.

Scheme II

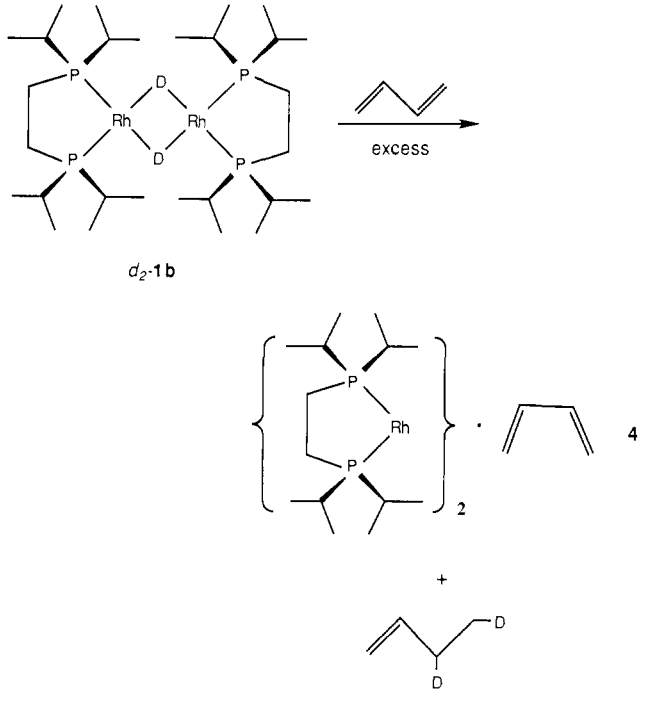

the results of this X-ray analysis with the solution spectroscopic data from the dippp reaction was the composition of **4** unraveled.

Solid-State Molecular Structure of $[(dippe)Rh]_2\cdot C_4H_6$. The molecular structure obtained through X-ray analysis of single crystals of **4** is as shown in Figure 2. Figure 2A shows the structure and atom numbering scheme, while Figure 2B is a stereoview of the molecule. There are two dimeric molecules per asymmetric unit, each having similar bond distance and bond angle parameters (Table VI) (supplementary material). The C_4H_5 ligand is attached to Rh(1) in a cis-η^4 fashion and σ-bonded to Rh(2) via C(91), thus bridging the two metal centers in a previously unreported mode of bonding.[12] The Rh(1) center has a distorted square-pyramidal geometry, with the bridging hydride occupying the apical position, while the geometry at Rh(2) is nearly square planar.

The interatomic rhodium–carbon distances in this structure compare favorably with similar parameters found for the $\mu\text{-}\eta^2\text{-}\sigma$ vinyl hydride complex $[(dippe)Rh]_2(\mu\text{-}\eta^2\text{-}\sigma\text{-}CH{=}CH_2)(\mu\text{-}H)$[16] in which the vinyl ligand bridges the two rhodium centers in a mode analogous to C(91) and C(92) in **4**. In addition, the Rh–Rh separation of 2.8105 (8) Å in **4** is just slightly shorter than that of 2.8655 (5) Å found in the vinyl hydride complex. Rhodium–phosphorus distances and angles in **4** are also comparable and unremarkable.

The bridging hydride ligand was located and refined isotropically and was found to bridge the two metal centers symmetrically, unlike the hydride ligand in the vinyl hydride complex. The C–C distances in the dienyl ligand of **4** are all virtually identical at 1.40 Å, indicating complete π-delocalization over the diene ligand.

Solution-State Molecular Structure of $[(dippe)Rh]_2\cdot C_4H_6$. In solution, the complex of the formula $[(dippe)Rh]_2\cdot C_4H_6$ is in fact an equilibrium mixture of the dienyl hydride dimer **4a** and the partial sandwich complex **4b** (eq 1). The van't Hoff plot of the temperature dependence (above −20 °C) of the equilibrium constant is shown in Figure 3; Table IX lists a number of temperatures and the value of the equilibrium constant (defined by

Table IX. Values of the Equilibrium Constant K and $\Delta G°$ as Defined by Equation 1

temp, °C	K_{eq} = [**4b**]/[**4a**]	$\Delta G°$, cal/mol
18.9	0.27	771.4
30.8	0.33	676.1
40.7	0.39	583.4
45.8	0.42	546.0
50.7	0.46	498.5
60.9	0.54	412.4
70.9	0.62	330.7

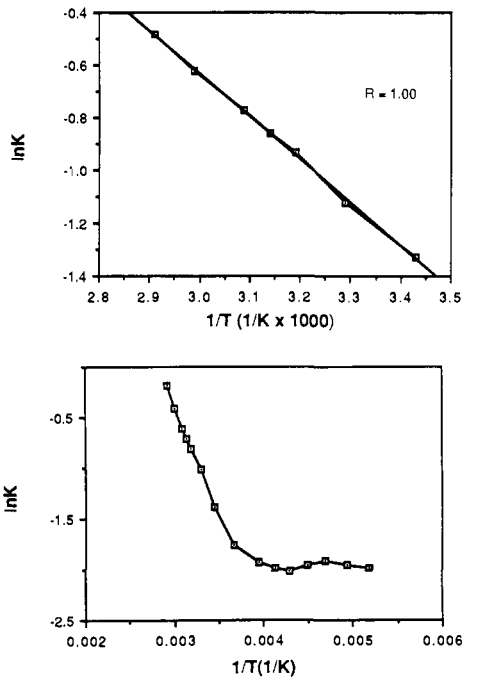

Figure 3. (a, top) van't Hoff plot of the equilibrium between the butadienyl–hydride **4a** and the partial sandwich species **4b** in C_7D_8 (linear region). (b, bottom) The same plot over the full measured temperature range showing the lack of change in K below −20 °C.

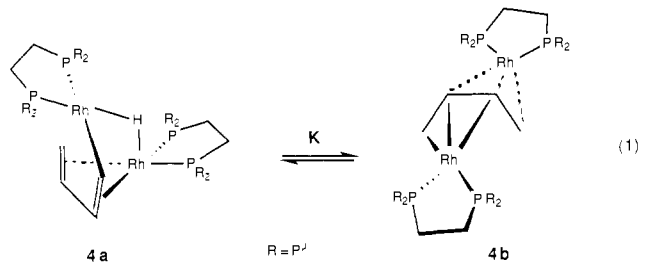

(1)

K = [**4b**]/[**4a**]) along with the values of $\Delta G°$. Graphically determined thermodynamic parameters for eq 1 are $\Delta H° = 3.3 \pm 0.1$ kcal/mol, and $\Delta S° = 8.5 \pm 0.2$ cal/mol. Below −20 °C, the equilibrium is halted.

The origin of the complexity of the dippe reaction with 1,3-butadiene was only apparent once the $^{31}P\{^1H\}$ NMR spectrum of **4** was measured at 121 MHz and compared to the spectrum of the dippp sandwich **2**; initial $^{31}P\{^1H\}$ NMR spectra of **4** at lower field (32.4 MHz) were uninterpretable. The diagnostic, temperature-independent AA′BB′XX′ pattern of **2** mentioned previously was evident in the $^{31}P\{^1H\}$ NMR spectrum of **4** along with a more complex temperature-dependent pattern; a series of these spectra are shown in Figure 4. The ^1H NMR spectrum of the mixture of **4a** and **4b** consists of the characteristic resonances for the diene protons of **4b** and other broad, featureless peaks associated with **4a**; no fine structure or coupling patterns are discernable for **4a** even with selective ^{31}P decoupling. A hydride multiplet is evident at −8.26 ppm and is assigned to **4a**. All of the ^1H NMR resonances associated with **4a** are temperature dependent. The $^{13}C\{^1H\}$ NMR spectrum of **4** can be assigned. At low temperature (−70 °C), four resonances due to the dienyl carbons of **4a** are observed at 156.9 (multiplet, C_1, σ-bound to Rh), 123.5 (s, C(2)), 88,8 (s, C(3)) and 33.1 ppm (s, C(4)); in addition, the two temperature-independent multiplets for the diene carbons of **4b** are also apparent. As the temperature is raised, the two inner carbons of **4a** at 123.5 and 88.8 ppm broaden and coalesce to a broad peak at approximately 106 ppm; the remaining two resonances for the terminal carbons are barely observable due to broadening.

Because of the temperature dependence and the complexity of the ^1H, $^{13}C\{^1H\}$, and $^{31}P\{^1H\}$ NMR spectra for **4a**, the solution structure of this dienyl–hydride may not have the C_4H_5 fragment bound in the μ-η^4-σ form as found in the solid state. In fact, the only convincing evidence for this formulation is the presence of the hydride multiplet in the ^1H NMR spectrum, which distinguishes this binding mode from the μ-η^3-η^3 type for **4b**. At low temperatures, this μ-η^4-σ mode is certainly a possibility as it is consistent with all of the spectroscopic data; however, there may be other formulations for **4a**. For example, dissociation of one end of the π-bound diene to generate a μ-η^2-σ dienyl–hydride is attractive, since it is known that analogous μ-η^2-σ alkenyl–hydride complexes can undergo a "windshield wiper" fluxional process.[16] However, this type of fluxional behavior alone is not sufficient to fully account for the temperature dependence of the solution spectra. The variable-temperature $^{31}P\{^1H\}$ NMR spectra shown in Figure 4 require a process or series of processes that make all four phosphorus and both rhodium nuclei equivalent in the fast-exchange limit. In the low-temperature limit, the complexity of the $^{31}P\{^1H\}$ NMR spectra is consistent with a structure like the μ-η^4-σ mode or perhaps the μ-η^2-σ type. Whatever process is invoked must also satisfy the $^{13}C\{^1H\}$ NMR results wherein the inner carbons of the dienyl ligand exchange in the fast-exchange limit; presumably the terminal carbons are also exchanging in this process. In addition, the observation that the dienyl–hydride complex **4a** and the partial sandwich **4b** are in equilibrium must also be broached. Indeed, the temperature dependence of the solution spectra suggests that this complex **4** is undergoing quite massive structural rearrangements.

Scheme III presents two possible scenarios to the explain the exchange processes of the complexes **4a** and **4b**. The interconversion of the μ-η^4-σ form (A) with the μ-η^2-σ mode (B) does not exchange any of the carbons of the dienyl unit nor does it make the phosphorus environments identical; the two rhodium centers are exchanged, however. To accomplish the interchange of carbons, two possible transformations are reductive elimination from A to the cis diene C or hydride migratory insertion to the double bond of B to give F. In both the diene manifold (C, D, and E) and the μ-butenediyl manifold (F and G), the interchange of rhodium centers, phosphorus donors, and carbon nuclei is achieved. There is ample precedent (see introduction) for the proposed structures having a cis-bound diene to one metal of a cluster (i.e., C, C′, D, and D′) and the μ-η^2-η^2-cis form in E. Analogy for the μ-η^3-σ structure (i.e., F) is also available with $(CO)_5Mn(\mu\text{-}\eta^3\text{-}\sigma\text{-}C_4H_6)Mn(CO)_4$,[33] while G has some precedent in $[(CO)_5Re]_2(\mu\text{-}\sigma\text{-}\sigma\text{-}C_4H_6)$.[34] The rearrangement of the μ-1,2-butenediyl form F to the μ-1,4-butenediyl structure G is attractive, as this allows easy conversion to the partial sandwich product **4b** by coordination of the double bond to the two unsaturated rhodium centers. Although the accessibility of the partial sandwich complex via G might tend to disfavor the diene manifold, it should be noted that E can be converted to G by interaction of the electron density of the Rh–Rh bond with the 1,3-butadiene π-system, as shown in eq 2. This corresponds to a 4 + 2 cy-

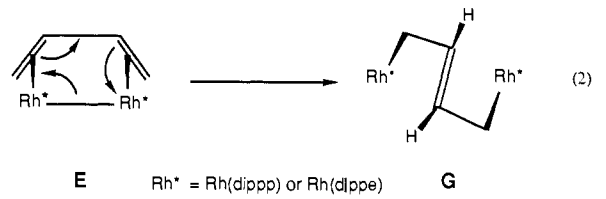

E Rh* = Rh(dippp) or Rh(dippe) G (2)

cloaddition and has precedent[35] in related 2 + 2 additions of olefins with photochemically generated $Os_2(CO)_8$, a molecule with a formal osmium–osmium double bond (Os=Os).

The equilibrium between the dienyl hydride **4a** and the partial sandwich **4b** favors the dienyl–hydride (eq 1). The rate of this transformation is extremely slow since sharp signals for **4b** are observed at all temperatures irrespective of the fluxional behavior of **4a**. Indeed, at −20 °C, this equilibrium is completely halted. Integration of the respective resonances ($^{31}P\{^1H\}$ NMR spectrum) of the two species below −20 °C shows no shift in equilibrium even after several hours.

The Magnesium Butadiene Reaction. The unusual nature of the binuclear products obtained from the reaction of 1,3-butadiene with the hydride dimers **1a** and **1b** provided the incentive to examine other possible synthetic routes to these materials. One rational sequence that proved successful was the reaction of "magnesium butadiene" ($[Mg{\cdot}C_4H_6{\cdot}2THF]_n$) with the chloro-bridged dimers of rhodium as shown in eq 3 and 4. Typically,

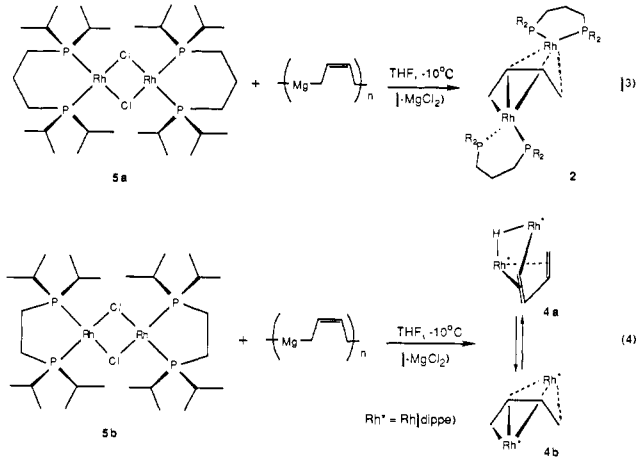

(3)

(4)

the $[P_2Rh](\mu\text{-}Cl)_2$ derivatives were dissolved or suspended in THF,

(33) Kreiter, C. G.; Lipps, W. *Angew. Chem., Int. Ed. Engl.* **1981**, *20*, 201.
(34) Beck, W.; Raab, K.; Nage, U.; Sacher, W. *Angew. Chem., Int. Ed. Engl.* **1985**, *24*, 505.
(35) Hember, R. T.; Scott, C. P.; Norton, J. R. *J. Am. Chem. Soc.* **1987**, *109*, 3468.

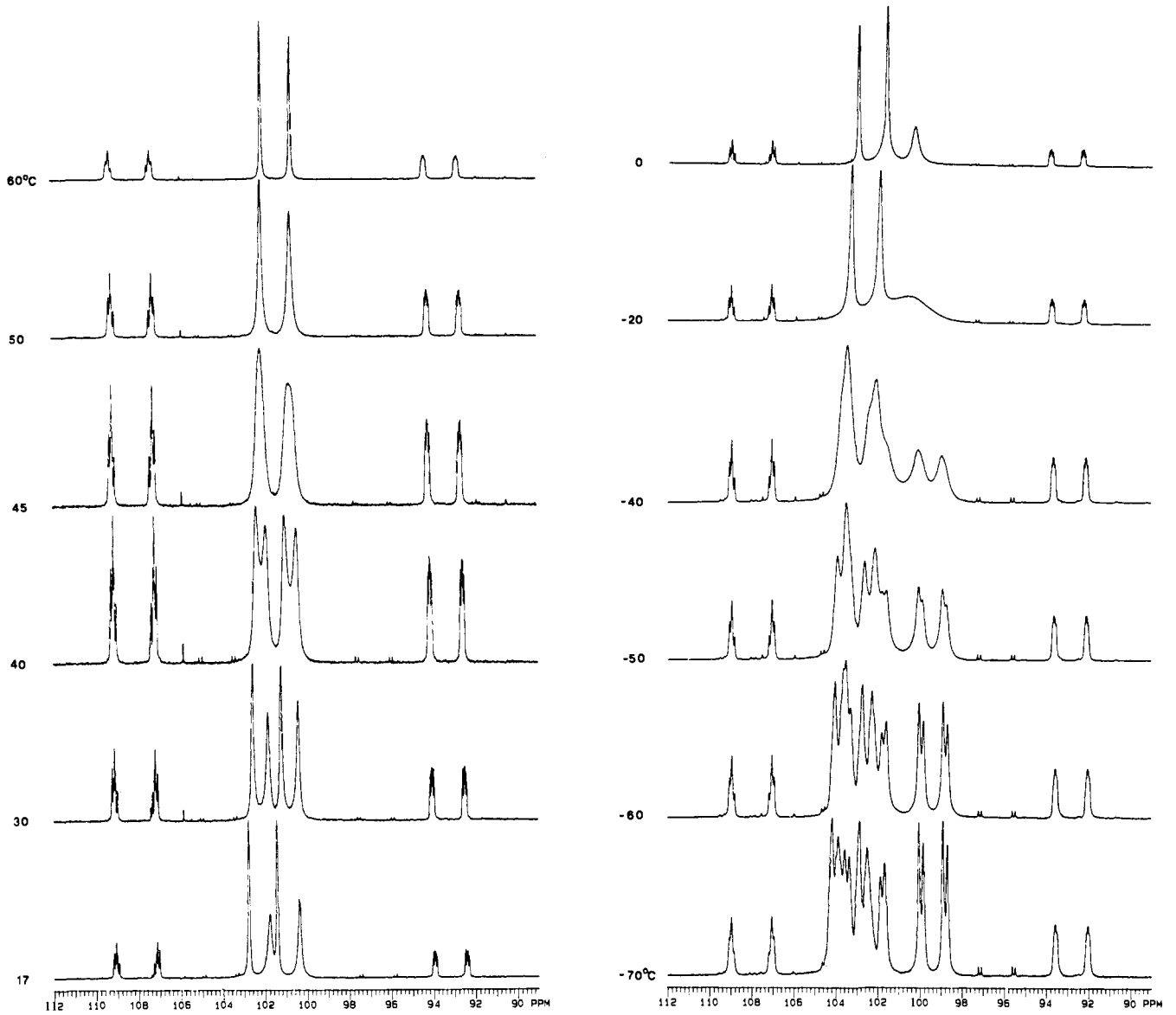

Figure 4. $^{31}P\{^1H\}$ NMR spectra (C_7D_8, 121.421 MHz) of the equilibrium mixture of **4a** and **4b** at a variety of temperatures. The temperature-dependent pattern in the center of each spectrum is due to **4a**, while the outside, temperature-independent multiplets are due to **4b**.

cooled to −10 °C, and solid magnesium butadiene added all in one portion. The products were obtained in excellent yield after workup.

This procedure is the method of choice for the preparation of the dippp partial sandwich **2** since the yield is virtually quantitative and no mononuclear allyl side products are obtained. Interestingly, the reaction of the dippe rhodium chloride-bridged dimer leads to the equilibrium mixture of **4a** and **4b** in reasonable yield. Although we are still in the process of examining the generality of this procedure, the reaction of magnesium butadiene with a number of other rhodium chloride-bridged dimers incorporating chelating electron-rich phosphine ligands does generate the binuclear butadiene structures found for the dippp and dippe dimers, including those derivatives for which hydride dimers are not easily accessible.[36]

Based on literature precedent,[37] the mechanism of this reaction probably involves stepwise metathesis of the bridging chlorides by the bifunctional "butadiene" Grignard. This generates the already proposed (Scheme III) intermediate F, which can rearrange to G; both F and G are pivotal to the proposed mechanism of formation of binuclear products as discussed in a following section.

The Purple Intermediate. When the reaction of $[(dippe)Rh]_2(\mu\text{-}H)_2$ (**1b**) with excess (2–5 equiv) 1,3-butadiene is conducted at temperatures lower than −40 °C, a transient purple color is observed. By maintaining the temperature at −80 °C, a deep purple solution is obtained that persists to about −50 °C, whereupon it fades to the orange color of the products. If the 1,3-butadiene is pumped off under vacuum at ≤−60 °C, the purple solution reverts back to the deep-green color of the starting dihydride **1b**. At these low temperatures, this purple intermediate can be isolated as a dark purple crystalline solid that decomposes to a green-orange material above −20 °C, perhaps indicating a disproportionation to **1b** and products. In our hands this thermal instability precluded any solid-state structural analysis but did allow solution spectroscopic data to be collected.

The ^1H, $^{31}P\{^1H\}$, and $^{13}C\{^1H\}$ NMR spectra are indicative of a highly asymmetric structure and consistent with one end of the 1,3-butadiene π-bound to one rhodium center of the hydride dimer, as shown in **6**. All four phosphorus nuclei are inequivalent as judged by the complexity of the $^{31}P\{^1H\}$ NMR spectrum. The ^1H NMR spectra at low temperatures (≤−60 °C) show six sep-

(36) (a) The dihydride dimer $[(dtbpp)Rh]_2(\mu\text{-}H)_2$, where dtbpp = 1,3-bis(di-*tert*-butylphosphino)propane, was not accessible via normal preparative routes. However, the chloro-bridged analogue was readily available, and reacted with magnesium butadiene to give the partial sandwich derivative containing dtbpp in excellent yield.[36b] (b) Fryzuk, M. D.; Piers, W. E. *Polyhedron* **1988**, *6*, 1001.

(37) Erker, G.; Krüger, C.; Müller, G. *Adv. Organomet. Chem.* **1985**, *24*, 1.

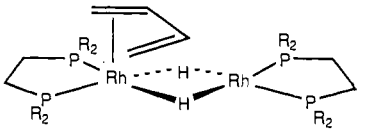

6

arate proton resonances for the butadiene; although the resonances are broad, a combination of homonuclear and heteronuclear (^{31}P) decoupling experiments established the connectivity and the fact that the diene was cis bound ($^3J_{H_3,H_4}$ = 5 Hz).[26] The $^{13}C\{^1H\}$ NMR spectra also support the structure **6** as four separate carbon resonances for the butadiene moiety are also observed. The η^2-bound cis butadiene is rather labile, since even at −60 °C magnetization transfer between the diene protons on the η^2-bound ligand and free butadiene is observed upon homonuclear decoupling of the dienyl ligand resonances.

The analogous reaction of the dippp dimer $[(dippp)Rh]_2(\mu\text{-}H)_2$ (**1a**) with 1,3-butadiene is much slower and no corresponding purple intermediate was detected.

Mechanism of Formation of Binuclear Rhodium Butadiene Complexes. In this section, a discussion of the possible details of the reaction of 1,3-butadiene with the binuclear hydrides **1a** and **1b** is presented. The observation of binuclear products in both reactions suggests that binuclear intermediates are potentially involved. Although the rates of the reaction of 1,3-butadiene with each of the hydride dimers are quite different, as are the product distributions, a common mechanism will be assumed. At critical points in the proposed sequence, literature precedent is cited to provide evidence for particular intermediates.

The results of the reaction of the dideuterides (**1a**-d_2 and **1b**-d_2) with 1,3-butadiene clearly establish that the first equivalent of butadiene merely serves to dehydrogenate the hydride dimers. This is summarized in Scheme IV. Once the η^2-diene intermediate H is formed, insertion of the diene into the bridging hydride to generate the binuclear 1-methylallyl–hydride I followed by a binuclear reductive elimination of butene to generate the rhodium(0) dimer J is plausible. The μ-allyl intermediate has precedent from binuclear palladium complexes of the type $[(R_3P)Pd]_2(\mu\text{-}C_3H_5)(\mu\text{-Cp})$.[38] In the dippe sequence, the insertion and reductive elimination processes might be quite fast since only 1-butene is detected as a side product. By contrast, the analogous dippp reaction must be sufficiently slow to allow isomerization of I to K, which upon reductive elimination generates isomerized butenes. In addition, if the reductive elimination from I or K is indeed slow in the dippp reaction, a further insertion of butadiene can be invoked that will lead to the mononuclear allyl products **3a** and **3b**.

The rest of the reaction mechanism hinges on the rhodium(0) dimer J. Reaction of J with butadiene allows access into the diene manifold already discussed in the fluxional process of **4a**. Once E is formed, the subsequent transformations to G and on to the partial sandwich derivatives **2** and **4b** are analogous to that described for Scheme III. In addition, the μ-1,4-butenediyl dimer G can be rearranged to the μ-1,2-butenediyl dimer F, which after β-elimination generates the dienyl–hydride species A. Again the importance of the purported intermediates F and G is apparent since both of the observed types of binuclear products, the dienyl–hydride and the partial sandwich, emanate from them. That F and G can be accessed from the magnesium butadiene reaction with the chloro-bridged dimers is further support for this part of the mechanism.

The rhodium(0) dimer J is an interesting molecule. While we have been unsuccessful so far in synthesizing this type of coordinatively unsaturated d^9–d^9 dimer,[39] there is some precedent for its existence in the isolation and X-ray crystal structure of the d^{10}–d^{10} platinum dimer $[(dtbpp)Pt]_2$ [dtbpp = 1,3-bis(di-*tert*-butylphosphino)propane].[40] Extended Hückel calculations on this platinum dimer suggest that, in the planar geometry, the HOMO is antibonding (πd^*).[41] Given that J has two fewer electrons (d^9–d^9 vs d^{10}–d^{10}), the rhodium(0) dimer should be stabilized with respect to the platinum(0) dimer electronically. In fact, the frontier orbitals of J would be isolobal[41] with ethylene and provide further support for the conversion of purported E to G via a quasi 4 + 2 reaction as shown in eq 2 above. Another theoretical analysis for the hydride dimer $[\{(Pr^iO)_3P\}_2Rh]_2(\mu\text{-}H)_2$[42] gives an analysis for the Rh_2P_4 core that is similar to the Pt_2P_4 core discussed above.

The equilibrium between the dienyl–hydride **4a** and the partial sandwich **4b** obtained in the dippe reaction is more clearly delineated in Scheme IV. Dissociation of the π-bond of the sandwich to generate the μ-1,4-butenediyl dimer G, followed by rearrangement to F and subsequent β-elimination, produces the dienyl–hydride. The effect of the chelate ring size may be steric in origin since the larger six-membered chelate ring of the dippp ligand forces the isopropyl methyls more toward the Rh–Rh core of the binuclear unit than does the dippe ligand. In the dienyl–hydride structure, the central core is already crowded, thus destabilizing this isomer for the dippp system. In the dippe system, the slight thermodynamic preference for the dienyl–hydride **4a** over the partial sandwich **4b** is not easily justified.

Theoretical Analysis of the Bonding in the Partial Sandwich Structure. The unique nature of the partial butadiene sandwich structure found for both **2** and **4b** prompted us to more closely examine its bonding from a theoretical point of view.

From the crystal structure, the mode of bonding is μ-η^3-η^3. As a starting point, let us ask the question "why not a structure of the type μ-η^4-η^4" as shown in **7**. An orbital interaction diagram

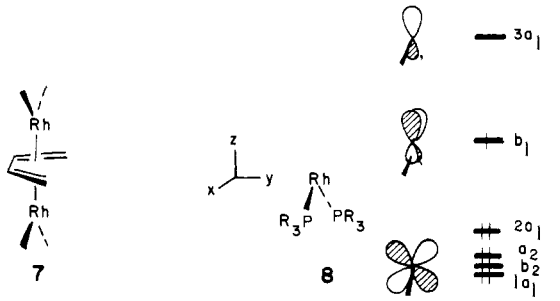

7 8

for **7** is easily constructed. The splitting pattern for a C_{2v} $Rh(PR_3)_2$ fragment[1] is given in **8**. Three orbitals, b_2, b_1, and $3a_1$, will figure heavily into the discussion and their shapes are explicitly drawn in **8**. At low energy, b_2 is one of four nonbonding d orbitals and is of metal *yz* character. The b_1 orbital is primarily *xz* on Rh antibonding to the phosphine σ-donor functions. Thus, it lies at a much higher energy than the other four orbitals. Furthermore, it is hybridized away from the phosphines by mixing *in* some Rh *x* character. At still higher energy is a Rh sp hybrid, $3a_1$. In analogy with **2**, the Rh–Rh distance in **7** should be approximately 4.12 Å. Thus, the orbitals of a $(R_3P)_2Rh\cdots Rh(PR_3)_2$ unit will be simple symmetric (S) and antisymmetric (A) combinations not split much in energy, as shown on the right side of Figure 5. On the left side are the four π-orbitals of butadiene. The lowest level, π_1, is stabilized by the A combination of $3a_1$. π_2 is stabilized by the A combination of b_1. Finally, π_3 and the A combination of b_2 interact to a smaller extent for overlap reasons (b_2 is not hybridized). All other orbitals are basically nonbonding, including the six symmetry-adapted combinations of $1a_1$, a_2, and $2a_1$ (see **8**), which are not shown in Figure 5. The resultant molecular orbitals are labeled according to C_{2v} symmetry in the molecule.

Notice that there is a very small energy difference between the molecular $3b_1$ and b_2 levels. Our extended Hückel calculations,

(38) Werner, A.; Kühn, A. *Angew. Chem., Int. Ed. Engl.* **1977**, *16*, 412.
(39) A cyclic voltammagram of the chloro-bridged dimer **5b** revealed a reduction occurring near the solvent limit. A variety of reducing agents were employed in an attempt to reduce **5b**, but only when Na/K was used did any reaction occur. Workup provided a red crystalline product, which decomposed rapidly at room temperature.
(40) Yoshida, T.; Yamagata, T.; Tulip, T. H.; Ibers, J. A.; Otsuka, S. *J. Am. Chem. Soc.* **1978**, *100*, 2063.
(41) Dedieu, A.; Hoffmann, R. *J. Am. Chem. Soc.* **1978**, *100*, 2074.
(42) Teller, R. G.; Williams, J. M.; Koetzle, T. F.; Burch, R. R.; Gavin, R. M.; Muetterties, E. L. *Inorg. Chem.* **1981**, *20*, 1806.

Scheme III

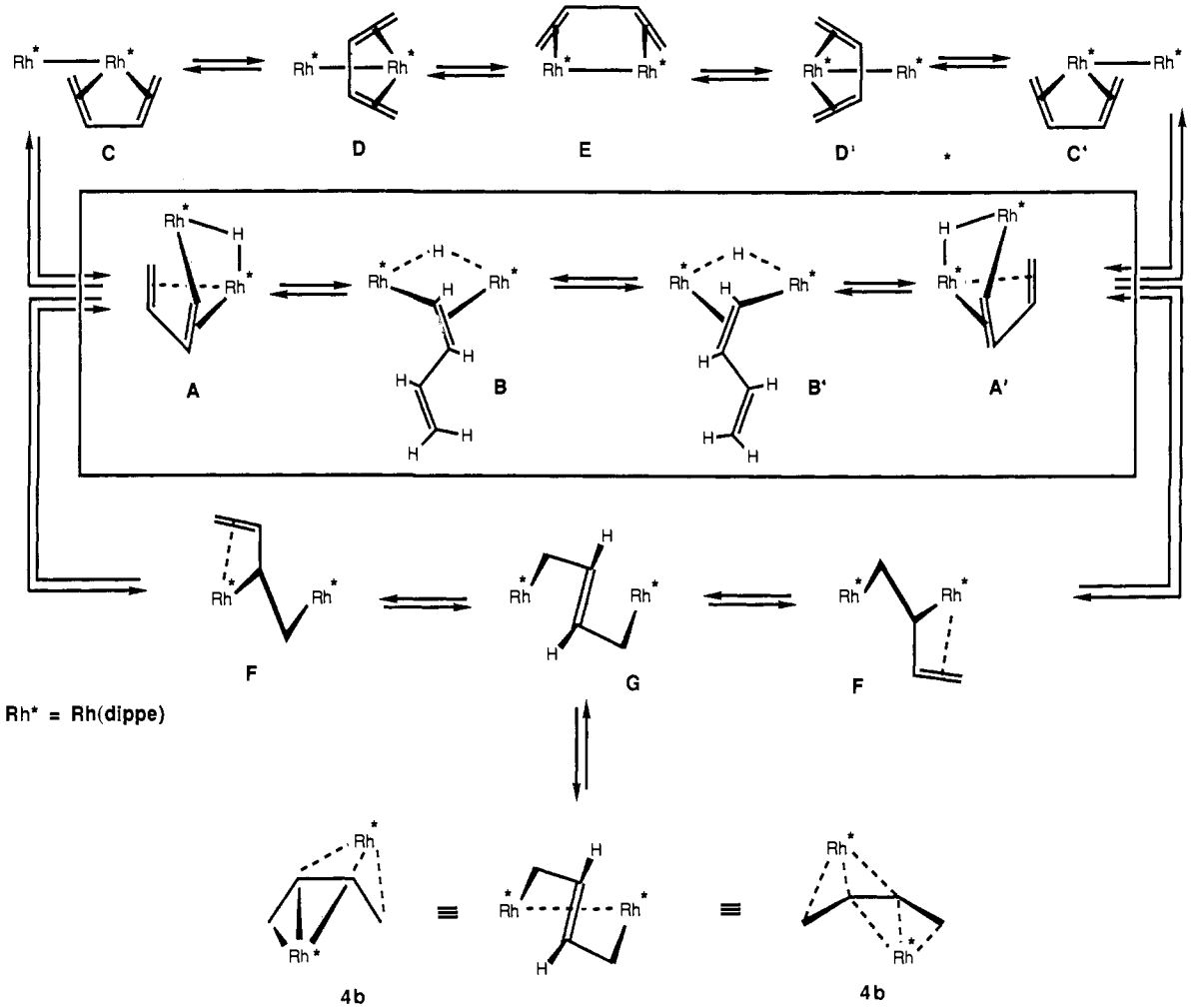

with computational and geometrical details given in the Experimental Section, but the $3b_1$ orbital slightly lower than b_2. Occupation of $3b_1$ and $2b_1$ means that in a formal sense π_3 on the butadiene fragment is occupied. Consequently, all three C–C distances are expected to be approximately equal—a feature that persists in the experimental structure for **2**. The existence of the low-lying b_2 molecular orbital is precisely analogous to that found for triple-decker Cp_3M_2 and CpM_2L_6 complexes,[43] which also can possess as many as four extra electrons. Regardless of whether $3b_1$ or b_2 are filled, the fact that there is little energy difference between them signals a possible second-order Jahn–Teller distortion[1] of $b_1 \times b_2 = a_2$ symmetry. A normal coordinate of this symmetry type is rotation of each $Rh(PR_3)_2$ unit in opposite directions, as shown in **9**, where θ measures the rotation of each

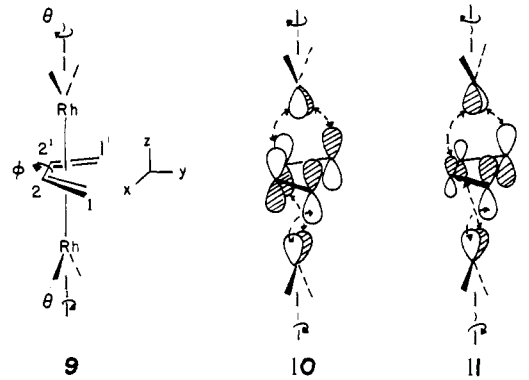

9 **10** **11**

P–Rh–P plane out of the xz plane. At $\theta = 0$, the overlap between the S combination of b_1 and π_3 (see Figure 5) is zero; however, increasing θ turns on overlap shown by the dashed arrows in **10**. Another way of putting this is that the a_2 motion reduces the molecular symmetry to C_2. Molecular $3b_1$ and b_2 now both have symmetry and consequently can mix, stabilizing the lower filled molecular orbital and destabilizing the upper empty one. Increasing θ to $\approx 45°$ will only slightly decrease the overlap between the A combination of b_1 and π_2 as shown in **11**.

A Walsh diagram, which shows the energetic variation of the six lowest molecular orbitals in Figure 5 with respect to rotation, is presented in Figure 6. Notice that as θ increases, the b_2–$3b_1$ separation increases dramatically, as expected from **10**. The 1_{a_2} orbital (see **11**) is actually stabilized. The reason behind this is that 1_{a_1} and 1_{a_2} mix into each other as θ increases. The latter is stabilized and the former is destabilized by this mixing. The optimum geometry occurs at $\theta = 48°$, i.e., close to where the two P–Rh–P planes are orthogonal. This structure is computed to be 35.2 kcal/mol lower in energy than **7** with $\theta = 0°$. There is another way to view this structural distortion. Consider butadiene to be a six π electron donor (with π_3 filled). Each $Rh(PR_3)_2$ unit then has a low-lying acceptor orbital, b_1 (see **8**), and maximal stabilization will occur when the acceptor functions are orthogonal, stabilizing π_2 and π_3, rather than when they are parallel and compete with each other for π_2. This is a general phenomenon found in many types of organic and inorganic molecules.[44] We shall return to a very closely related example shortly. Notice that irrespective of the value of θ, the occupancy of π_3 is close to two

(43) (a) Lauher, J. W.; Elian, M.; Summerville, R. H.; Hoffmann, R. *J. Am. Chem. Soc.* **1976**, *98*, 3219. (b) See: Reference 1, pp 392–4.

(44) (a) Burdett, J. K.; Albright, T. A. *Inorg. Chem.* **1979**, *18*, 2112. (b) Reference 1, pp 285–8. (c) Rösch, N.; Hoffmann, R. *Inorg. Chem.* **1974**, *13*, 2656.

Scheme IV

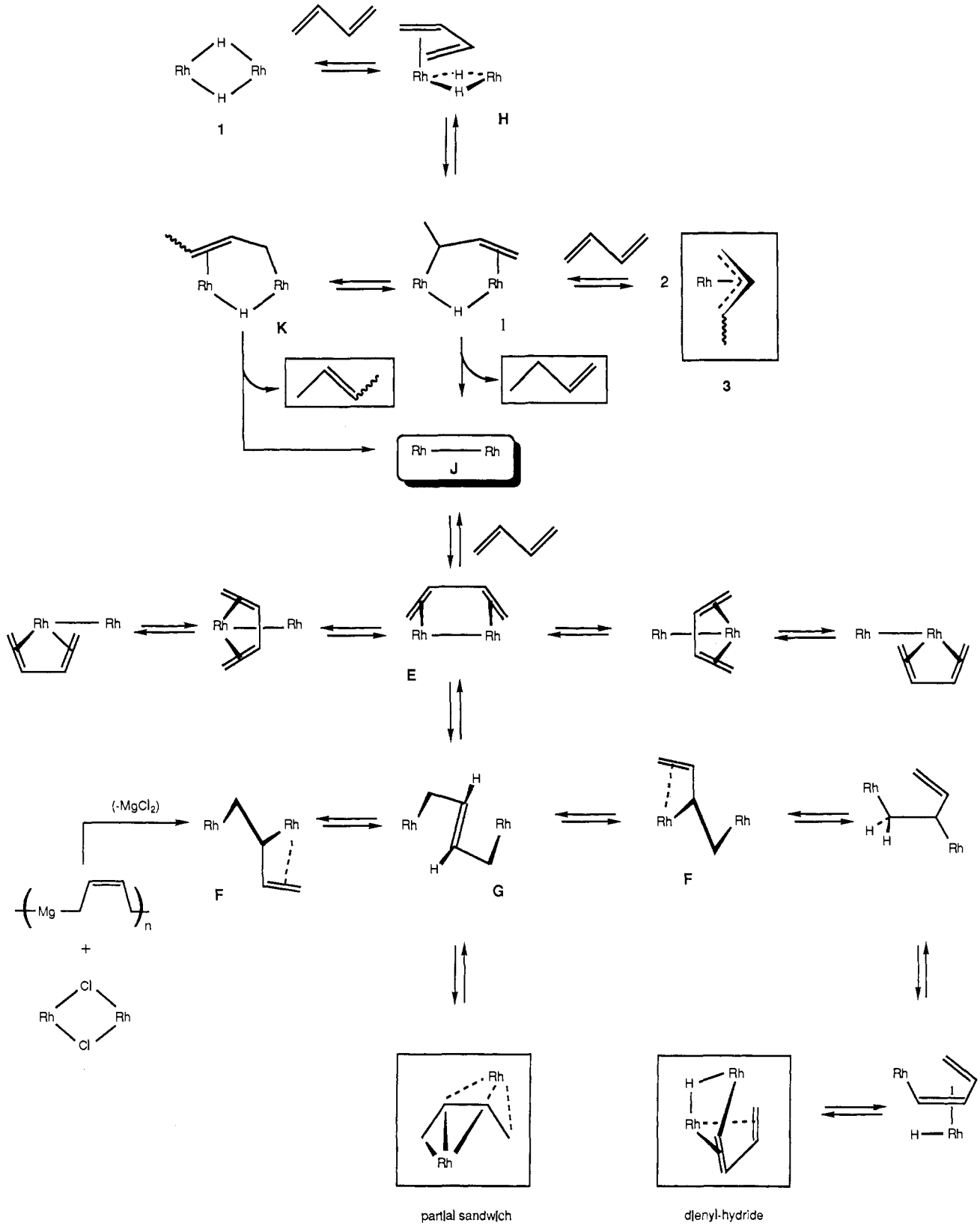

electrons, and therefore, alternation of the C–C bond lengths in the butadiene ligand is greatly reduced.

At the μ-η^4-η^4 point with $\theta = 50°$ the Rh–C overlap population is as follows: Rh(1)–C(1) = 0.145, Rh(1)–C(2) = 0.141, Rh(1)–C(2′) = 0.079, and Rh(1)–C(1′) = 0.034. The bonding between Rh(1) and C(1′) [along with that between Rh(1) and C(1)] is small as expected by **10** and **11**. Rotation of the two $Rh(PR_3)_2$ units provides the electronic genesis of μ-η^3-η^3 bonding. Rotation about the C(2)–C(2′) axis, ϕ in **9**, provided an optimized structure of $\theta = 45°$ and $\phi = 27°$, which was 13.5 kcal/mol lower in energy than that for $\theta = 48°$ and $\phi = 0°$. The experimental values for **2** are $\theta = 37.8°$ and $\phi = 45.0°$. The potential energy surface in this region is very soft; it requires only 4.3 kcal/mol to reach the experimental structure. Increasing ϕ serves to reorient the p atomic orbitals on C(2) and C(2′) so that bonding between π_3 and the S combination of b_1 is increased. At the optimum

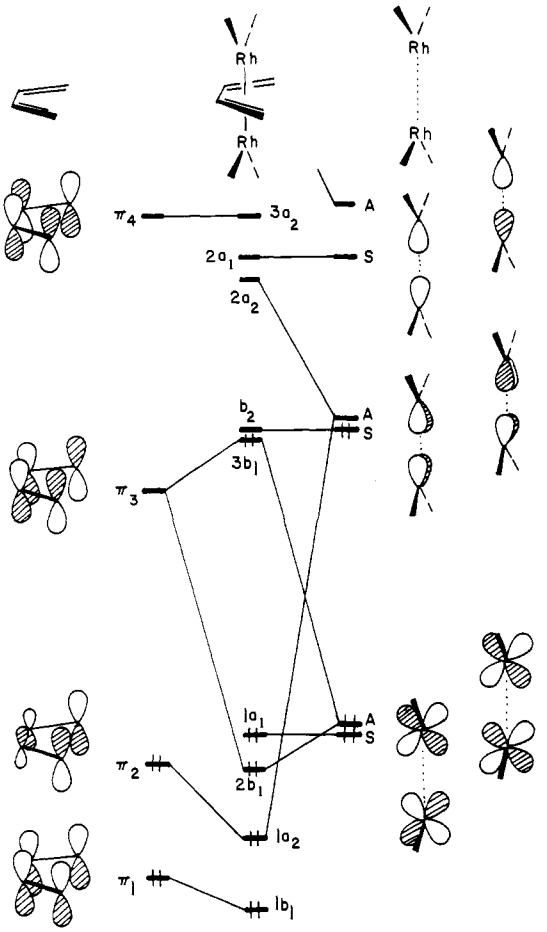

Figure 5. Orbital interaction diagram for the eclipsed molecule $[(R_3P)_2Rh]_2(\mu\text{-}\eta^4\text{-}\eta^4\text{-}C_4H_6)$ **7**.

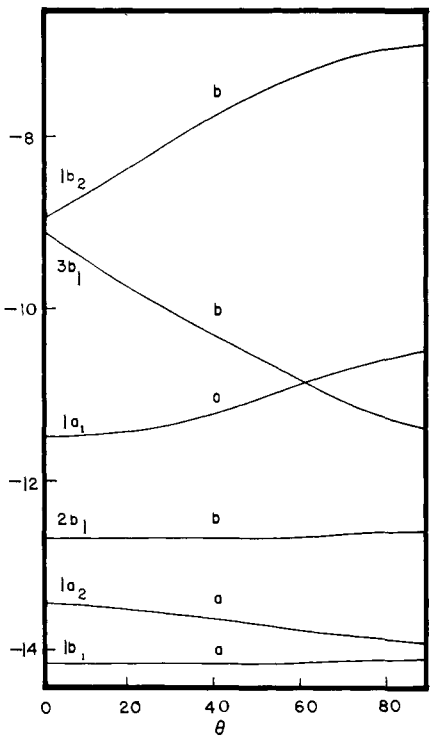

Figure 6. Walsh diagram for rotation of the $Rh(PR_3)_2$ units, θ, defined in **9**. The energy scale on the left is in electronvolts.

structure the Rh–C overlap populations are Rh(1)–C(1) = 0.205, Rh(1)–C(2) = 0.147, Rh(1)–C(2′) = 0.112 and Rh(1)–C(1′) = −0.025. Notice that each Rh atom is coordinated in an η^3 mode, furthermore, the $Rh(PR_3)_2$ unit is more strongly bonded to the end carbon atom, primarily because of the polarization in π_2. This reproduces the observed asymmetry of the Rh–C bond lengths in **2**.

Another possible structural type for a partial sandwich type complex was investigated by considering the bridging C_4H_6 fragment in a trans conformation. Extended Hückel calculations were carried out on **12** to test this hypothesis. At a symmetrically

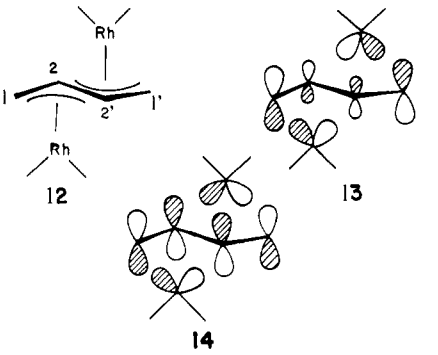

coordinated $\mu\text{-}\eta^3\text{-}\eta^3$ geometry, **12** was found to lie only 4.3 kcal/mol above the optimized structure of **10**. At this geometry the two $Rh(PR_3)_2$ units are predicted to lie parallel to each other. The A combination of b_1 stabilizes π_2, **13**, while the S combination stabilizes π_3, **14**. The polarization in π_2 again favors asymmetric bonding; the Rh–C overlap populations were Rh(1)–C(1) = 0.210, Rh(1)–C(2) = 0.136, and Rh(1)–C(2′) = 0.129. Thus, we predict that the Rh(1)–C(1) distance should be shorter than that for Rh(1)–C(2′). Notice from **14** that rotation about the C(2)–C(2′) axis will be destabilizing. A sizable activation energy would therefore exist for the conversion of **12** into E or the partial sandwich structure **2**, and this can account for its unavailability.

The $\mu\text{-}\eta^3\text{-}\eta^3$ mode of bonding in **2** is really a byproduct of the fact that the set of b_1 acceptor levels on the $Rh(PR_3)_2$ units prefer to be orthogonal. There is nothing particularly wrong with $\mu\text{-}\eta^4\text{-}\eta^4$ coordination by itself. Consider $[(PR_3)_2Rh]_2(C_4H_4)$ at a D_{2d} geometry which is shown, along with a Newmann projection, in **15**. A simplified interaction diagram for this molecule is given

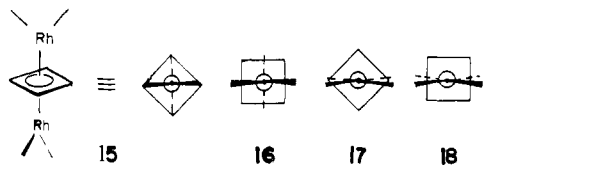

on the left side of Figure 7. The A combination of $Rh(PR_3)_2$ $3a_1$ hybrids stabilizes the lowest π-level of cyclobutadiene. The two b_1 orbitals form an e set, which stabilizes the middle two π-levels on cyclobutadiene. A large HOMO–LUMO gap computed for this hypothetical molecule implies reasonable stability. We also have examined distortions of **15** toward a $\mu\text{-}\eta^3\text{-}\eta^3$ coordination. All were found to be destabilizing. Notice that there is little difference in the bonding description for $[(PR_3)_2Rh]_2(C_4H_4)$ at **15**, which one would call $\mu\text{-}\eta^4\text{-}\eta^4$, and that for $[(PR_3)_2Rh]_2(C_4H_6)$ at $\theta = 45°$, which is $\mu\text{-}\eta^3\text{-}\eta^3$.

A further interesting feature in $[(PR_3)_2Rh]_2(C_4H_4)$ concerns its rotational barriers. There is essentially free rotation of the cyclobutadiene ligand relative to the rest of the molecule. Rotation by 45° to **16** requires only 0.4 kcal/mol. At **16** a linear combination of the cyclobutadiene e set generates a new e set that will overlap with the b_1 acceptor functions to an identical extent. If, however, one $(PR_3)_2Rh$ unit is rotated by 90°, then the situation is radically altered. In either **17** or **18** the molecular symmetry is D_{2h}. The S combination of b_1 hybrids now has b_{2u} symmetry and is left nonbonding; see the right side of Figure 7. Likewise, one component of the cyclobutadiene e set has b_{2g} symmetry and is left nonbonding. The A combination of b_1 functions and one component of the cyclobutadiene π-set both have b_{3g} symmetry

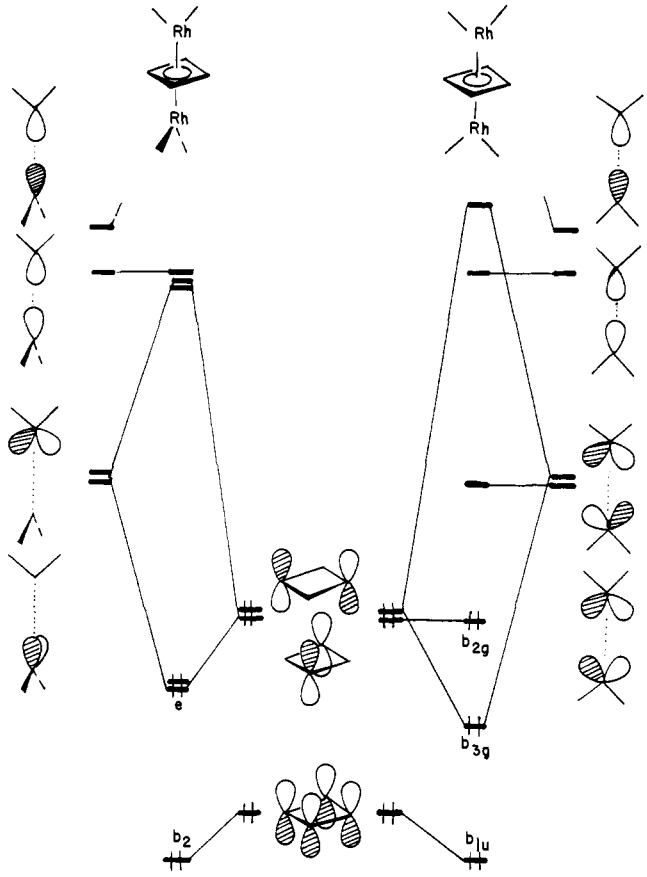

Figure 7. Orbital interaction diagram for both the staggered (**15**) and eclipsed (**17**) forms of $[(R_3P)_2Rh]_2(\mu\text{-}\eta^4\text{-}\eta^4\text{-}C_4H_4)$.

and one bonding molecular orbital is created. It can be shown from perturbation theory arguments[44] that the *net* stabilization of two electrons in molecular b_{3g} (right side of Figure 7) is less than the stabilization of four electrons in the molecular e set (left side of Figure 7). Thus, there is a very large barrier upon rotation from **15** to **17** or **16** to **18** (33.9 and 32.6 kcal/mol, respectively).

Conclusions

The result of the reaction of a *mononuclear* transition-metal hydride with 1,3-butadiene is fairly straightforward and predictable. Either one obtains a simple adduct of the diene and the hydride, or further insertion to generate 1-methylallyl complexes is observed. In this study, the *binuclear* rhodium complexes $[\{Pr^i_2P(CH_2)_nPPr^i_2\}Rh]_2(\mu\text{-}H)_2$ (n = 3, **1a**; n = 2, **1b**), having bridging metal hydrides, form binuclear complexes of the general formula $[\{Pr^i_2P(CH_2)_nPPr^i_2\}Rh]_2\text{-}C_4H_6$ as the major product upon reaction with 1,3-butadiene; labeling studies indicate that the bridging hydrides are removed in an initial step, presumably generating a reactive, unsaturated binuclear intermediate that binds butadiene to generate the isolated products.

The major product upon reaction of $[(dippp)Rh]_2(\mu\text{-}H)_2$ (**1a**) with 1,3-butadiene has the butadiene intact and *partially sandwiched* in a $\mu\text{-}\eta^3\text{-}\eta^3$ bonding mode between two skewed (dippp)Rh units. A theoretical analysis of the bonding in **2** indicates that the skew is a result of the acceptor orbitals of the separated (dippp)Rh fragments preferring to be orthogonal. In fact, analysis of the as yet unknown molecule $[(R_3P)_2Rh]_2(C_4H_4)$ (**15**), having the cyclobutadiene sandwiched between the two $(R_3P)_2Rh$ fragments, indicates that the $\mu\text{-}\eta^4\text{-}\eta^4$ bonding mode is most stable with completely staggered P_2Rh units. However, in the partial sandwich complex **2**, the skewed and twisted geometry observed is found to be the more stable than an eclipsed $\mu\text{-}\eta^4\text{-}\eta^4$ form by 48.7 kcal/mol.

The analogous reaction of 1,3-butadiene with $[(dippe)Rh]_2(\mu\text{-}H)_2$ (**1b**), generates the complex **4**, which is in fact an equilibrium mixture of two binuclear products: the butadienyl–hydride **4a**, having a $\mu\text{-}\eta^4\text{-}\sigma\text{-}C_4H_5$ unit resulting from C–H activation of butadiene, and the partial sandwich analogue of **2** above, **4b**. The solution behavior of these two complexes is extremely complex. Not only are these two derivatives in dynamic equilibrium above −20 °C, but **4a** is undergoing some fluxional process that symmetrizes the complex in the high-temperature limit. To account for the massive structural rearrangements in solution, a fluxional process is proposed (Scheme III) that satisfies all of the observations by invoking reversible C–H bond activation as a key step in the scheme.

The binuclear complexes **2** and **4a** can also be accessed by the use of magnesium butadiene with the corresponding chloride-bridged dimers **5**. This transformation provides some insight into the mechanism of formation of these complexes, as shown in Scheme IV. Indeed, many of the steps proposed in Scheme IV have precedent as detailed in an earlier section.

The results of this study underscore the ability of more than one metal center to engage in new bonding schemes with small organic molecules. In addition, the rearrangement of the 1,3-butadiene moiety on two rhodium centers is remarkable and should be a feature of other extended π-systems with these reactive dirhodium cores.

Acknowledgment. Financial support for this work was provided by NSERC of Canada (operating grants to M.D.F. and F.W.B.E.; postgraduate scholarship to W.E.P.), the Robert A. Welch Foundation (T.A.A.), and by the donors of the Petroleum Research Fund (T.A.A.), administered by the American Chemical Society, for support of this work. We are grateful for a generous allocation of computer time by NSF at the Pittsburgh Supercomputing Center. Johnson Matthey is also gratefully acknowledged for the loan of $RhCl_3$ (MDF).

Supplementary Material Available: Tables II–VI, XI–XIII, XV, and XVI containing anisotropic and isotropic thermal parameters, calculated hydrogen parameters, and bond lengths and angles for **2** and **4a** and annular torsion angles and torsion angles for **2** (17 pages); Tables XIV and XVI containing observed and calculated structure factors for **2** and **4a** (141 pages). Ordering information is given on any current masthead page.